POLITECNICO
MILANO 1863

SCUOLA DI INGEGNERIA INDUSTRIALE
E DELL'INFORMAZIONE

A novel approach for Camera - Laser line calibration

Tesi di Laurea Magistrale in
Music and Acoustic Engineering - Ingegneria Musicale E Acustica

Author: **Haokun Song**

Student ID: 10680040
Advisor: Prof. Marco Marcon
Co-advisors: Marco Compagnoni
Academic Year: 2019-2023

Abstract

The accurate calibration of camera-laser systems is essential for various computer vision applications, such as 3D reconstruction, object recognition, and robotics. This thesis presents a comprehensive investigation into the extrinsic calibration of camera-laser systems, aiming to enhance the accuracy and efficiency of the calibration process. The research begins with a comprehensive literature review, examining existing extrinsic calibration methods and mathematical models for both camera and laser sensors. Various techniques for establishing correspondences between camera and laser data are explored and categorized, establishing a strong theoretical foundation for the subsequent calibration methodologies. The first phase of the research focuses on the modeling of the camera and laser systems. Mathematical formulations are derived to describe the geometric relationship between the 3D world coordinates and the corresponding image or laser points. The camera model is based on the classical pinhole camera model, while the laser model incorporates parameters for range and intensity measurements. Next, the thesis delves into the extrinsic calibration procedure. The process involves estimating the rotation matrix and translation vector that defines the rigid transformation between the camera and laser coordinate systems. Various calibration patterns, including checkerboards and laser lines, are utilized to establish correspondences between the two sensors. The thesis presents a novel calibration framework that combines feature-based correspondence analysis and optimization algorithms. This framework leverages the rich geometric information captured by the camera and the line-laser sensor to accurately estimate the transformation parameters. Experimental evaluations are conducted using a custom calibration setup, validating the effectiveness and accuracy of the proposed framework. Furthermore, the thesis explores the impact of different factors on calibration accuracy, including noise, distortion, and environmental conditions. Robustness analysis and sensitivity studies are performed to evaluate the resilience of the calibration methods under challenging scenarios. The findings of this research contribute to the advancement of camera-laser extrinsic calibration techniques, offering practical insights and recommendations for achieving precise alignment in real-world applications. The proposed methodologies serve as a reliable foundation for accurate perception and measurement tasks.

Keywords: computer vision, extrinsic calibration, camera-laser systems, plücker matrix, optimization algorithms, calibration accuracy, 3d reconstruction, robustness analysis.

Abstract in lingua italiana

La calibrazione accurata dei sistemi fotocamera-laser è essenziale per varie applicazioni di visione artificiale, come la ricostruzione 3D, il riconoscimento di oggetti e la robotica. Questa tesi presenta un'indagine completa sulla calibrazione estrinseca dei sistemi fotocamera-laser, con l'obiettivo di migliorare l'accuratezza e l'efficienza del processo di calibrazione. La ricerca inizia con una revisione completa della letteratura, esaminando i metodi di calibrazione estrinseca esistenti ei modelli matematici sia per i sensori a fotocamera che laser. Vengono esplorate e classificate varie tecniche per stabilire le corrispondenze tra i dati della fotocamera e del laser, stabilendo una solida base teorica per le successive metodologie di calibrazione. La prima fase della ricerca si concentra sulla modellazione della telecamera e dei sistemi laser. Vengono derivate formulazioni matematiche per descrivere la relazione geometrica tra le coordinate del mondo 3D e l'immagine o i punti laser corrispondenti. Il modello della fotocamera si basa sul classico modello della fotocamera stenopeica, mentre il modello laser incorpora i parametri per le misurazioni della portata e dell'intensità. Successivamente, la tesi approfondisce la procedura di calibrazione estrinseca. Il processo prevede la stima della matrice di rotazione e del vettore di traslazione che definisce la trasformazione rigida tra la telecamera e i sistemi di coordinate laser. Vari modelli di calibrazione, tra cui scacchiere e linee laser, vengono utilizzati per stabilire corrispondenze tra i due sensori. La tesi presenta un nuovo framework di calibrazione che combina analisi delle corrispondenze basate su caratteristiche e algoritmi di ottimizzazione. Questo framework sfrutta le ricche informazioni geometriche acquisite dalla fotocamera e dal sensore laser lineare per stimare con precisione i parametri di trasformazione. Le valutazioni sperimentali vengono condotte utilizzando un'impostazione di calibrazione personalizzata, convalidando l'efficacia e l'accuratezza del framework proposto. Inoltre, la tesi esplora l'impatto di diversi fattori sull'accuratezza della calibrazione, inclusi rumore, distorsione e condizioni ambientali. Vengono eseguiti analisi di robustezza e studi di sensibilità per valutare la resilienza dei metodi di calibrazione in scenari difficili. I risultati di questa ricerca contribuiscono al progresso delle tecniche di calibrazione estrinseca laser-fotocamera, offrendo spunti pratici e raccomandazioni per ottenere un allineamento preciso nelle applicazioni del mondo reale. Le metodologie proposte fungono da base af-

fidabile per compiti di percezione e misurazione accurati.

Parole chiave: visione artificiale, calibrazione estrinseca, sistemi camera-laser, matrice di plücker, algoritmi di ottimizzazione, accuratezza della calibrazione, ricostruzione 3d, analisi di robustezza.

Contents

1 | Introduction

1.1. Overview and Motivation

The usage of camera and laser systems has become increasingly common in various industrial and scientific applications, for instance, robotics, machine vision, 3D reconstruction, navigation systems, autonomous driving, and industrial automation. In order to ensure that the multiple-view measurement data from the camera and laser can be accurately fused and analyzed, it is essential to determine the relative position and orientation of the sensors, a process known as extrinsic calibration. By calibrating the extrinsic parameters, we can ensure that the camera and laser are correctly aligned, providing more accurate 3D data and improved results in various applications.

This thesis focuses on the extrinsic calibration of a camera and a laser, with the goal of determining the position/orientation of the laser laine relative to the camera. The proposed method to determine the position of the laser line involves intersecting the laser with a set of planar checkerboards of known dimensions which are applied as calibration object and they are actually completed with different postures on the same planar checkerboard. This approach provides us with the joint objective of calibrating the camera optics and determining the plane of the laser, thus allowing for the accurate mapping of 3D data in the real world.

In an ideal scenario, two images of the checkerboards in different positions would suffice to solve the problem of determining the plane of the laser, provided that the two planes of the checkerboards and the laser do not belong to the same beam of planes. However, in a real context, there are several sources of error and noise in the acquisition process that need to be addressed to minimize their impact on the accuracy of the results.

To validate the proposed method, an experiment was performed using the system of a real camera combined with a 2D laser sensor. This experiment involved the 3D reconstruction of a complex-surfaced trunk model using calibrated laser line data. The results of this experiment will demonstrate the effectiveness of the approach in providing a robust and efficient solution for the extrinsic calibration of the camera and the laser.

1.2. Organization of The Thesis

The remainder of this thesis is organized as follows: Chapter 2 provides a comprehensive review of prior research concerning the extrinsic calibration of camera-laser line systems. Following this, Chapter 3 delves into the mathematical foundations, notably Plücker matrices, fundamental to this project. This chapter also delves into critical aspects such as distortion and system stability. Subsequently, Chapter 4 provides a comprehensive account of the experimental setup, detailing the datasets, algorithms, procedures, and showcasing visual representations along with data analyses. Chapter 5 draws the work to a conclusion and outline potential areas for further research and development.

2 | Background and Related works

This chapter will provide an overview of the development of joint external calibration methods for cameras and other sensors, with a particular focus on laser in this article. The narrative commences by delving into seminal works, including traditional camera calibration, which serves as a catalyst for the subsequent discussion.

The primary objectives of this chapter are:

- provide a comprehensive understanding of the historical progression in joint extrinsic calibration methodologies that involve the alignment of cameras and laser. By examining the evolution of calibration techniques over time, this study seeks to shed light on the advancements made in achieving accurate spatial alignment between these two sensing modalities;
- To facilitate a better understanding of the available techniques, the existing extrinsic calibration methods of the camera-laser system will be categorized based on their fundamental principles and methodologies;
- To present state-of-the-art techniques for extrinsic calibration of cameras and laser, highlighting their distinct approaches and advancements.

2.1. Traditional Camera Calibration as a Precursor

In computer vision, one of the fundamental tasks is to derive the geometric information of objects in 3D space from the image data captured by cameras. This enables subsequent reconstruction and recognition of the objects. The geometric model of a camera determines the relationship between the 3D position of an object point in space and its corresponding projection in the image. This highlights the significance of the camera's geometric model, with the parameters encapsulated in the model referred to as camera parameters. The process of determining these parameters is known as camera calibration. To achieve 3D reconstruction, stereo vision methods typically involve three main steps. Firstly, the corresponding points between images need to be determined, establishing the relationship between the projection points of the same space point in different images.

Secondly, camera calibration is performed to determine the connection line between the image point and the camera's optical center. This step involves determining both the intrinsic and extrinsic parameters of the camera. Lastly, utilizing the camera's intrinsic and extrinsic parameters, along with the results of image matching, the 3D reconstruction is carried out. This process calculates the distance between the object and the camera, yielding comprehensive 3D information about the object. In this article, our primary focus is on the crucial step of camera calibration which is the process of mapping pixel coordinates of space points to their corresponding world coordinates and a vital process in 3D stereo vision that directly impacts the accuracy of the subsequent reconstruction results.

Camera calibration involves the determination of both intrinsic and extrinsic parameters of a camera based on the world coordinates of a reference point in space and its corresponding image coordinates.

Intrinsic Parameter Determination:

- Accurate estimation of the camera's intrinsic parameters is crucial for achieving precise calibration. The lens focal length(f), lens distortion coefficients(k, s, p), coordinate distortion factor(s), and image coordinate(u0, v0) origin play pivotal roles in accurately mapping image coordinates to their corresponding world coordinates. These parameters directly impact the geometric transformation between the real-world coordinate system and the image coordinate system. Thorough understanding and robust estimation of these parameters contribute to the improvement of image quality, accurate feature extraction, and reliable camera pose estimation.

Extrinsic Parameter Determination:

- Determining the extrinsic parameters of the camera is also crucial for establishing the relationship between the camera coordinate system and the world coordinate system. The rotation matrix R and translation vector t define the position and orientation of the camera in 3D space, enabling accurate registration of the captured images with the corresponding real-world objects or scenes. The determination of these parameters is essential for applications such as camera tracking, augmented reality, and robotics.

The common theory and methods of high-precision camera calibration are thoroughly discussed in [1], including the pinhole model which serves as a foundational concept in camera calibration, serving as a starting point for many advanced techniques. This simplified model assumes a small aperture and a single point of projection, providing a

simplified yet effective representation of the camera's imaging process. Virtually all advanced calibration techniques build upon the principles and concepts derived from the pinhole model. Its use as a foundation allows for the development of more sophisticated and accurate calibration methodologies.

Nowadays, the most widely used and representative calibration methods are the well-known Tsai's method [2, 3] and Zhang's method [4].

2.1.1. Tsai Camera Calibration Method

This method was first proposed by Tsai in 1986. Its implementation requires a minimum of six non-coplanar 3D points with known coordinates in the world coordinate system and their corresponding 2D pixel coordinates in the image. The two-stage technique employed in Tsai's method enables the separate determination of intrinsic and extrinsic parameters. In the first stage, the position and orientation of the camera are computed, establishing the camera's spatial relationship with the world coordinate system. This step provides the foundation for subsequent calibration procedures. In the second stage, the intrinsic parameters of the camera, including focal length and distortion coefficients, are calculated. By separating the calibration of intrinsic and extrinsic parameters, Tsai's method offers flexibility in adjusting camera settings and accommodating different imaging scenarios.

Furthermore, Tsai's method combines the advantages of the Direct Linear Transform (DLT) algorithm and nonlinear optimization techniques. The utilization of the DLT algorithm allows for the estimation of initial parameters, while the subsequent nonlinear optimization further refines the calibration to achieve greater accuracy. By transforming the nonlinear problem into the linear model, the calculation process is simplified, the calculation efficiency is improved, and the calculation result is more accurate. In the meanwhile, an important aspect of Tsai's method is its consideration of various distortions that can affect the camera's imaging process. Distortions such as lens distortion can introduce significant errors in the calibration results if not properly accounted for. By integrating distortion considerations into the calibration process, Tsai's method addresses this challenge and improves the accuracy of the calibration model. This enables more precise geometric reconstruction and accurate mapping between the real-world coordinates and the image coordinates. Tsai's method has proven to be an effective and valuable tool in the field of camera calibration.

2.1.2. Zhang Zhengyou Calibration Method

Zhang's algorithm has emerged as the most commonly employed method for camera calibration. This innovative approach addresses the challenges associated with radial distortion in camera parameters through the utilization of multi-plane images. The calibration process involves capturing multiple sets of images from various angles and directions using a printed checkerboard pattern. By analyzing the relationship between the feature points on the calibration pattern and their corresponding image points, namely the homography matrix of each image, the intrinsic and extrinsic parameters of the camera are constrained effectively. Then the maximum likelihood criterion is used to nonlinear optimize the calculated results, minimize the re-projection error(RPE) in the image space, and estimate the parameters of the pinhole model extended by some low-order polynomial distortion terms.

The canonical version of Zhang's algorithm requires a sparse set of point-like features with known relative 3D positions, which can be reliably identified in 2D images. Commonly used patterns include cell corners in a flat checkerboard pattern printed on a rigid surface. However, more advanced calibration patterns, such as fractals or complex star-shaped features, have been explored to reduce biases and enhance the robustness of feature detection [5, 6]. In some cases, advanced detection algorithms may introduce complexities in estimating residual localization errors. To mitigate these unknown errors, sophisticated procedures like minimizing discrepancies between recorded and inversely rendered pattern images have been employed [7]. However, it is important to note that despite these improvements, the sparse nature of the datasets is still preserved.

One notable advantage of Zhang's algorithm is the practicality and convenience it offers. The checkerboard pattern, which is the calibration pattern mentioned earlier, can be easily produced and reproduced by anyone. This approach combines high precision and good robustness, facilitating its widespread adoption worldwide. As a result, it has significantly accelerated the transition of 3D computer vision from laboratory research to real-world applications. The experiment in this article applied such a standard calibration checkerboard patter in Figure 2.1.

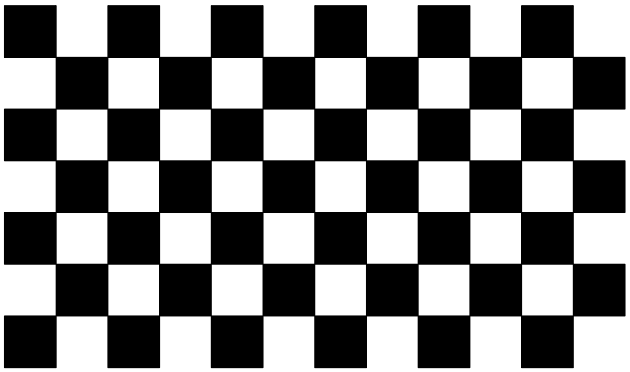

Figure 2.1: Standard Calibration Checkerboard Pattern.

2.2. Integration of Camera and Laser

This article builds upon traditional camera calibration techniques and focuses on the integration of camera and laser. Recognizing the inherent limitations of a single sensor, the adoption of multi-sensor fusion has emerged as a means to enhance system robustness. Leveraging a multi-sensor approach enables the mitigation of intrinsic drawbacks associated with individual sensors, leading to more reliable and comprehensive data acquisition. Extrinsic calibration procedures have been extensively explored in the literature, catering to the calibration of various configurations involving multiple laser units [8], multiple cameras [9], and different combinations of cameras and lasers. However, the majority of published calibration approaches have primarily concentrated on the extrinsic calibration of a single camera and laser unit. This article follows a similar setup, conducting the experiment based on this prevalent configuration.

A fundamental challenge lies in effectively matching data acquired by the distinct sensors. This difficulty can be mitigated if the geometric transformations between sensor frames are known. Extrinsic calibration plays a vital role in this regard, aiming to match and align the data provided by the camera and laser, thereby enabling the identification of the geometric transformation between these two sensors. Specifically, by deriving a closed-form solution for the relative orientation between the two sensors, it becomes feasible to linearly determine the translation. As a result, the rotation translation matrix between the two sensors can be obtained. This enables the fusion of data in a coherent 3D coordinate system.

Notably, the intrinsic parameters of the camera and the laser are assumed to be known, given that both have undergone prior calibration(Intrinsic Calibration).

Intrinsic Calibration of the Camera:

- The intrinsic parameters of the camera encompass the intrinsic matrix K and lens distortion parameters D. Typically, users can position the camera at various locations to observe a calibration object and utilize nonlinear optimization techniques to estimate K and D. This estimation process involves minimizing the re-projection errors of detected corner points obtained from checkerboard patterns [4]. By optimizing the intrinsic calibration, the camera's inherent properties can be accurately characterized.

Intrinsic Calibration of the Laser:

- In contrast to the camera, the intrinsic calibration of the laser presents additional complexity as it is intricately linked to the laser's mechanical structure. Consequently, these parameters are meticulously calibrated by the laser manufacturer. The intrinsic parameters of the laser, which remain constant during practical applications, play a crucial role in ensuring precise and consistent measurements.

While the laser sensor provides sparse yet precise depth information of the object or scene, the camera captures its rich 2D appearance and color details. These distinct types of information exhibit high complementarity, each possessing unique advantages, as well as inherent limitations. The essence of a multi-sensor fusion system lies in effectively learning from the strengths and weaknesses of each sensor, enabling a synergistic utilization of their respective data.

2.2.1. Evolution of Extrinsic Calibration Approaches for Camera and Laser

In 1995, Wasielewski and Strauss [10] proposed a calibration methodology specifically designed for integrating a monochrome charge-coupled device (CCD) camera and a 2D lidar sensor. This approach primarily relies on the constraints imposed by the projection of lines onto the camera image and the intersection points of these lines with the slice plane of the lidar sensor in the world coordinate system. The authors introduced a specific calibration pattern, comprising two intersected planes, to facilitate the alignment of data obtained from the camera and the lidar sensor, enabling the precise identification of the geometric transformation between the lidar and camera. The estimation of calibration parameters was achieved through the utilization of nonlinear least squares optimization techniques. However, it is important to acknowledge that the calibration errors were found to be influenced by the angle between the lines and the slice plane of the lidar sensor, a

factor that varied with different sensor positions.

Zhang and Pless [11] proposed a widely popular solution using a checkerboard for extrinsic calibration of a camera and a 2D laser sensor in 2004, marking a significant milestone in this field. During the multi-sensor extrinsic calibration procedure, the 2D laser sensor poses unique challenges due to its restricted field of view confined to 2D space, rendering its calibration more complex compared to the 3D laser sensor. This approach employs point-to-plane geometric constraints for extrinsic calibration, parameterizing the calibration pattern based on its unit normal vector and distance to the camera coordinate frame. For successful practical implementation, it is necessary to position a planar calibration pattern within the field of view of both the camera and the laser. This positioning ensures that the calibration pattern is visible to both sensors. Additionally, a minimum of five plane inputs (five planar shots) is required to complete the calibration process effectively. Initially, this solution minimizes an algebraic error which is the Euclidean distance between a planar pattern and the scan data is computed. Subsequently, to further refine the solution, the method employs a strategy of minimizing the re-projection errors, taking into account the requirement that the laser points should lie on this plane. This refinement process is carried out iteratively using advanced non-linear optimization techniques, allowing for an effective solution to be obtained.

However, this approach has limitations, as it solely focuses on the distance between laser points and the corresponding plane, and requires a significant number of diverse observations over a wide range. Simultaneously, a systematic study exploring the minimal solution to the original problem is lacking [12]. To address the limitations mentioned above, researchers have explored alternative solutions. The perspective-three-point (P3P) problem in [13] gives the minimum solution to the issue, Vasconcelos et al., deriving a minimal solution using only three planar shots. However, this method involves solving the sophisticated P3P problem in dual 3D space with eight solutions, thereby potentially encountering degeneration issues. In order to mitigate the degeneration problem, Hu et al. [14] proposed an alternative approach that relies on a single shot of a trirectangular trihedron calibration object. By solving simplified P3P and perspective-three-line (P3L) problems separately for the laser and camera poses, this method enables the derivation of a unique and accurate solution.

Similar to [11], the Unnikrishnan and Herbert method [15] solves the extrinsic calibration problem using plane-to-plane geometric constraints. A plane is fitted to the checkerboard in each coordinate frame and parameterized as a normal vector and a distance with respect to its origin coordinate frame. Later, the rigid body transformation between the two reference frames is estimated by minimizing the difference in orientation

and distance of the planes observed in each of the two coordinate systems.

In accordance with the proposed framework in the early stages, numerous research studies have been conducted to investigate various calibration methods for determining the parameters of the laser plane. It is important to highlight that all the aforementioned extrinsic calibration methods necessitate the usage of a calibration object, thereby falling under the category of *Target-Based Calibration Method* within the current extrinsic calibration domain. It is evident that the fundamental element of the *Target-Based Calibration Method* lies in the design of a specific target with well-defined structural characteristics, referred to as the calibration target. In practice, this method is typically implemented in a specified location and relies on one or more specialized calibration targets. These targets encompass a range of options, such as the planar checkerboard pattern [11, 13, 16], the V-shaped calibration target [10, 17], the simple circle [18, 19], or the planar board with circular holes [20], among others. When utilizing these diverse calibration targets, estimation of the rotation (R) and translation (T) parameters is facilitated through the application of the perspective-n-point (PnP) algorithm [21], direct linear transformation (DLT) method [22], and bundle adjustment (BA) algorithm [23]. The presence of the *Target-Based Calibration Method* naturally implies the existence of the *Targetless Calibration Method* and various other calibration approaches. The classification of various extrinsic calibration methods for camera and laser will be explored in Section 2.3.

2.3. Categorization of Existing Extrinsic Calibration Methods of Camera and Laser

Based on the requirement for calibration target, the process of extrinsic calibration between a laser sensor and a camera can be categorized into two main approaches: *Target-Based Method* and *Target-Less Method*. Moreover, these approaches can be further divided into two groups depending on the level of human intervention involved: *Manual* and *Automatic* methodologies. As indicated above, please consult Figure 2.2 for the categorization reference.

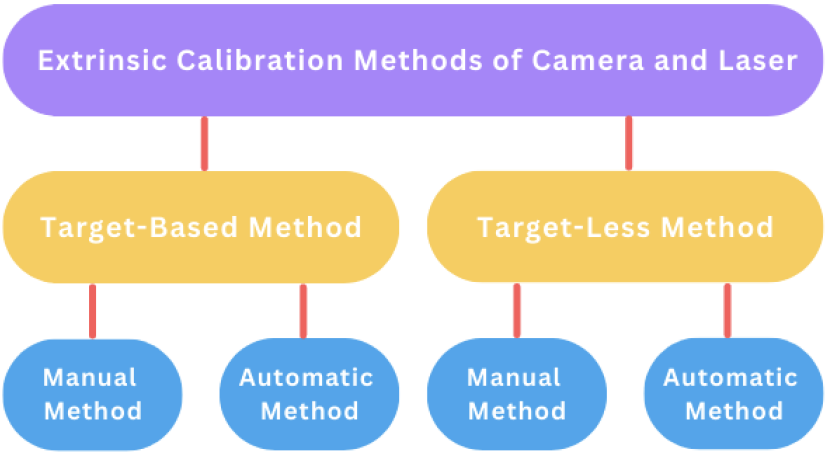

Figure 2.2: Categorization of Extrinsic Calibration Methods of Camera and Laser.

2.3.1. Manual Target-based Calibration Method

The *Target-Based Method*, as discussed in Section 2.2.1, involves the use of one or more artificial calibration targets. Multiple views of the target are typically required to extract feature correspondences between the laser and the camera. These correspondences serve as the basis for deriving geometric constraints, involving 3D points in point clouds and corresponding pixels in the image, in order to estimate the relative transformation between the sensors. The extraction of these feature correspondences can be performed either manually, with human intervention, or automatically, without requiring human involvement. Early studies, such as those conducted by Zhang and Pless [11] and Unnikrishnan and Herbert [15] employed manual extraction of features, representing the *Manual Target-Based Method*.

2.3.2. Automatic Target-based Calibration Method

Contrary to the *Manual Target-Based Method*, the *Automatic Target-Based Calibration Method* eliminates the need for human intervention. In this method, the calibration target is automatically detected, and correspondences between point clouds and images are estimated using diverse features related to the calibration target. Within this category, several calibration methods have been developed. Tulsuk et al. [24] presented a calibration method similar to Zhang and Pless [11], which utilizes automatic feature correspondence extraction. In this method, the extrinsic calibration parameters are refined by solving a non-linear least square problem, where the orthogonal distances between laser points and the 2D line (the intersection of the laser scan plane and checkerboard plane) were

minimized. Geiger et al. [16] introduced an automated method that only required a single shot. Specifically, the method involved identifying multiple checkerboards in different locations instead of capturing multiple shots of a single checkerboard placed in varying positions.

However, the automatic calibration method faces challenges in handling low-density laser information for extrinsic calibration, as it requires relatively dense 3D points in point clouds to match corresponding pixel data in the image. Additionally, automatic methods are primarily effective in structured scenes, such as specially designed environments, and may yield suboptimal results in natural environments. Therefore, the manual calibration method remains effective in ensuring robust operation across diverse scenarios.

2.3.3. Manual Target-less Calibration Method

As its name implies, the *Target-Less Method* involves does not rely on any calibration target to establish correspondences between features, such as edges, lines, and corners, extracted from both the laser and camera systems. It instead utilizes natural scene features to estimate the rigid transformation between the coordinate frames. Subsequently, the re-projection error associated with these correspondences is minimized. Within this category, the *Manual Target-Less Calibration Method* is distinguished by its reliance on human intervention to localize feature correspondences from the natural scenes. As stated above, this method eliminates the need for artificial calibration targets in the laser and camera coordinate frames. In practical implementation, this method typically requires the utilization of a predetermined set of rules or patterns.

In 2007, Scaramuzza et al. [25] introduced a *Manual Target-Less Calibration Method*. The method involves a step-by-step procedure to establish point correspondences between 3D points in point clouds and pixels in images, forming point-to-point geometric constraints. Once the point correspondences are identified, the extrinsic parameters, representing the rigid transformation between the two reference frames, are estimated using the widely-used PnP (Perspective from n Points) algorithm. Subsequently, an iterative least-squares refinement is applied to enhance the accuracy of the calibration results.

2.3.4. Automatic Target-less Calibration Method

The *Manual Method* face substantial challenges in accurately identifying 3D point features in laser data, a task that proves to be considerably more complex compared to identifying their correspondences in images. Additionally, uncertainties in the laser data introduce measurement errors, compromising the reliability of the calibration procedure. To im-

prove these limitations, the *Automatic Method* are necessary to enhance the calibration procedure.

The *Automatic Target-Less Calibration Method* aim to enhance the calibration procedure by either relying on extracted feature correspondences (point-to-point) from observed natural scenes to establish geometric constraints or utilizing motion information from the sensors to estimate the calibration parameters. This approach eliminates the need for specified calibration targets and reduces the reliance on manual intervention, thus streamlining the calibration process. Gomez-Ojeda et al. [26] introduced an *Automatic Target-Less Calibration Method* for the alignment of an LRF (Laser Range Finder) and a camera, utilizing both line-to-plane and point-to-plane geometric constraints. Notably, their method does not require the presence of any artificial calibration pattern. Instead, it relies on the detection of orthogonal trihedrons, commonly observed as scene corners in various human-made environments.

Furthermore, the *Automatic Target-Less Calibration Method* have found wide application in numerous practical scenarios involving autonomous systems. In this context, Rodriguez-Garavito et al. [27] proposed a extrinsic calibration method that leverages the simultaneous observation of a flat surface, typically a road, and an obstacle on the road, using both LRF and stereo camera sensors. The authors employed the M-estimator-Sample-Consensus (MSAC) algorithm to detect the road plane and resolve the alignment between the point clouds obtained from both sensors, thereby estimating the necessary extrinsic calibration parameters.

2.4. Advancements and Emerging Calibration Technologies Associated with Laser Line

Due to its remarkable resistance to interference, rapid scanning capabilities, and high precision, the line laser technology has found extensive applications in various industrial robot fields. The line-laser system emits a laser beam, which forms a fringe projection on the surface of the object. Subsequently, the camera captures this laser stripe and extracts its center. Finally, the system converts pixel information into range data using the transformation matrix between the laser plane and the camera frame.

Calibrating the relationship between the camera and the laser line plane is of paramount importance for line-laser systems. This calibration process can be broken down into two key components: camera calibration and laser plane calibration. The camera calibration technology has been comprehensively introduced in Section 2.1 and is considered rela-

tively mature in the field. On the other hand, various research approaches have been explored to determine the parameters of the laser plane. These calibration methods can be broadly categorized into several types, including:

- *Vector Cross Product* [28]: This method calculates the normal vector of the light plane by taking the cross product of two non-parallel laser stripe vectors;
- *Solution of Linear Equations* [29]: Here, a linear relationship between 3-D points on the laser plane and their corresponding 2-D pixel points is established using a transformation matrix;
- *Cross Ratio Invariance* [30]: Cross ratio invariance properties are leveraged to derive 3-D points on the laser plane, allowing for the conversion of the transformation matrix into laser plane equation parameters;
- *Vanishing Points and Lines* [31]: Normal vectors of the laser plane are determined through knowledge of vanishing points and lines in computer vision;
- *Plücker Matrix* [32]: This method directly solves the light plane equation using the Plücker matrix. However, it should be noted that understanding the derivation of the Plücker matrix method can be challenging, as it requires a background in computer vision and matrix theory.

These diverse calibration techniques offer options for determining the laser plane parameters, each with its own advantages and complexities. The choice of method often depends on the specific requirements of the application and the available expertise. In this research, the Plücker matrix technique is employed for line laser system calibration. Notably, this method eliminates the need to obtain standard points on the light plane, thereby avoiding positioning errors associated with multiple spatial coordinate transformations. As a result, this technique offers high calibration accuracy.

However, it is important to acknowledge some limitations. While this method effectively reduces image noise caused by electronic equipment, challenges remain in addressing object occlusion and specular reflections, which can be difficult to eliminate. Additionally, in complex environments, misoperations may occur, restricting its application in such scenarios. Despite these limitations, the current calibration methods for line-laser systems align well with future imaging requirements.

Since most calibration errors are attributed to image processing, the denoising of laser images can significantly reduce these errors. Line laser systems find applications in specialized areas like forging measurement and welding seam tracking, where traditional image processing techniques may not meet precision requirements. In recent years, neural-

network-based denoising methods have emerged for various fields, yet their application to line laser systems remains relatively unexplored. Leveraging existing image denoising algorithms, particularly those based on neural networks and enhanced denoising techniques, is poised to play a pivotal role in advancing line laser imaging systems.

3 | Methodology

To establish data association between the two sensors which are the camera and the laser, the initial step involves acquiring data in both coordinate systems. This article focuses on utilizing the *Manual Target-Based Calibration Method*, which serves as the fundamental approach for this purpose. A checkerboard is employed as the calibration target due to its ease of fabrication and the ability to generate multiple correspondences between the camera and the laser by manipulating the position of the pattern. The camera efficiently samples the feature points on the checkerboard, while the laser sensor captures information about the scanning plane. This chapter provides a comprehensive description of the theoretical approaches and mathematical foundations utilized to accomplish the extrinsic calibration of a camera and a laser within the scope of this research.

3.1. Camera Model

One of the fundamental objectives of computer vision is to derive the geometric properties of objects in the 3D space based on the image information captured by a camera. This process involves reconstructing and identifying objects using the relationship between the 3D geometric position of a point on the surface of a space object and its corresponding point in the captured image. the correlation between the 3D information and the 2D information is determined by the geometric model of the camera, as depicted in Figure 3.1, and these geometric model parameters are camera parameters. The camera is modeled typically represented using the classical pinhole camera model, which is based on **three elementary transformations**.

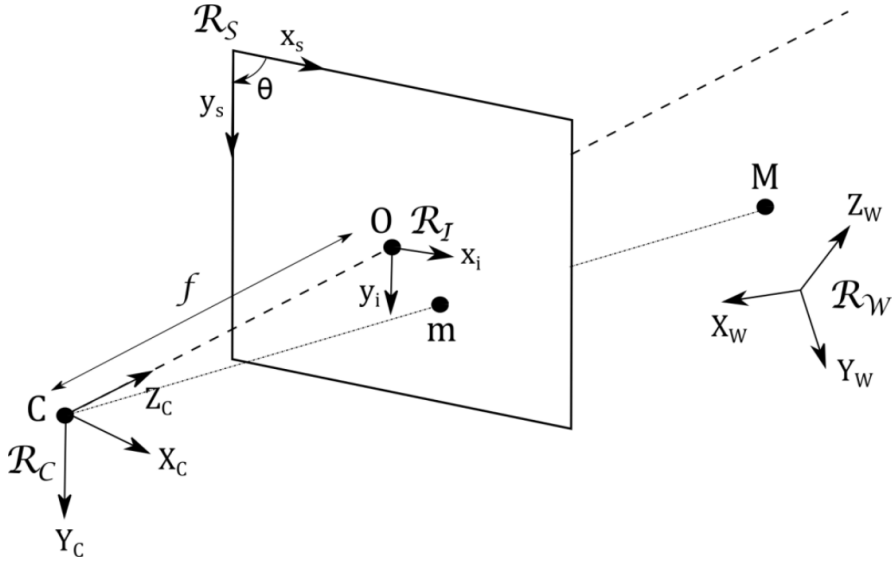

Figure 3.1: The Pinhole Camera Model [33].

Let $\boldsymbol{M} = [\mathrm{X_W}, \mathrm{Y_W}, \mathrm{Z_W}]^{\mathrm{T}}$ represent a point in the 3D world reference frame R_W, and $\boldsymbol{C} = [\mathrm{X_C}, \mathrm{Y_C}, \mathrm{Z_C}]^{\mathrm{T}}$ represent a point in the camera coordinate system R_C. The point $\boldsymbol{C}$ can be projected onto a pixel $\boldsymbol{O} = [\mathrm{x_i}, \mathrm{y_i}]^{\mathrm{T}}$ in the image frame R_I. This change of coordinate constitutes the **first transformation**, which is characterized by three rotations and three translations.

Furthermore, we denote $\hat{\boldsymbol{M}} = [\boldsymbol{M}^{\mathrm{T}}, 1]^{\mathrm{T}}$ and $\hat{\boldsymbol{C}} = [\boldsymbol{C}^{\mathrm{T}}, 1]^{\mathrm{T}}$ as the 3D point with homogeneous coordinate in the world reference frame R_W and the camera coordinate system R_C, respectively. The first transformation between the $\hat{\boldsymbol{M}}$ and the $\hat{\boldsymbol{C}}$ is mathematically represented by a *2×2* matrix, denoted as $\boldsymbol{T}$:

$$\boldsymbol{T} = \begin{bmatrix} \boldsymbol{R} & \boldsymbol{t} \\ \boldsymbol{0} & \boldsymbol{1} \end{bmatrix} \tag{3.1}$$

where $\boldsymbol{R}$ represents a *3×3* orthonormal rotation matrix, which can be parameterized using three rotation angles. $\boldsymbol{t}$ represents a *3×1* translation vector defined by its three components. And $\boldsymbol{0}$ is the zero vector. They can be described as follows:

$$\begin{bmatrix} \boldsymbol{R} & \boldsymbol{t} \\ \boldsymbol{0} & \boldsymbol{1} \end{bmatrix} = \begin{bmatrix} r_{\boldsymbol{11}} & r_{\boldsymbol{12}} & r_{\boldsymbol{13}} & t_{\boldsymbol{x}} \\ r_{\boldsymbol{21}} & r_{\boldsymbol{22}} & r_{\boldsymbol{23}} & t_{\boldsymbol{y}} \\ r_{\boldsymbol{31}} & r_{\boldsymbol{32}} & r_{\boldsymbol{33}} & t_{\boldsymbol{z}} \\ \boldsymbol{0} & \boldsymbol{0} & \boldsymbol{0} & \boldsymbol{1} \end{bmatrix} \tag{3.2}$$

The six parameters above comprising three rotation angles and three translations are commonly referred to as *Extrinsic Matrix/Parameters*. In the context of traditional single-camera calibration, the extrinsic parameters define the positioning of the camera in 3D space. However, in the case of multi-sensor calibration, such as combining the camera with the laser, the extrinsic parameters take on a different significance. In this scenario, the extrinsic parameters define the rigid transformation that establishes the spatial relationship between the various sensors involved. For this experiment, the latter scenario was adopted, focusing on the calibration of the camera-laser system and the estimation of its extrinsic parameters, please refer to Figure 3.2 for visual reference.

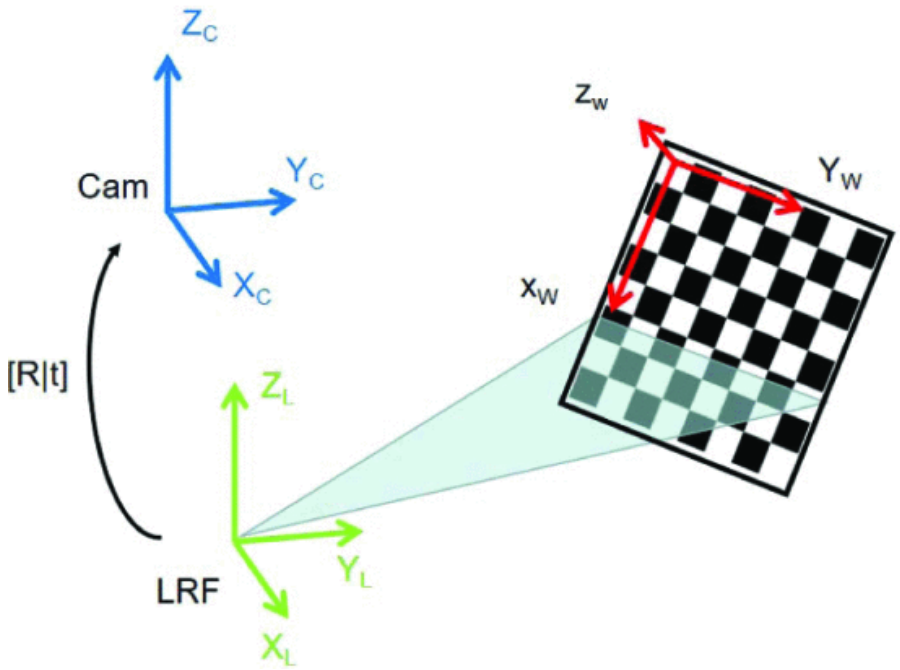

Figure 3.2: The Extrinsic Calibration of The Camera-Laser System.

Let $\mathbf{L} = [\mathrm{X_L}, \mathrm{Y_L}, \mathrm{Z_L}]^{\mathrm{T}}$ represent a 3D point in the reference coordinate system corresponding to the laser body frame R_L. This point is referred to as a "laser point" which is one of the points on the intersection line between the checkerboard and the laser in the context of this research article. As previously discussed, The rigid transformation from the laser coordinate system to the camera coordinate system can be represented by the following equation:

$$\boldsymbol{C} = \boldsymbol{R} \cdot \boldsymbol{L} + \boldsymbol{t} \tag{3.3}$$

Obviously, the extrinsic calibrations for the two sensors is to determine $\boldsymbol{R}$ and $\boldsymbol{t}$ from the

feature correspondences captured by the two sensors.

The **second transformation** corresponds to projecting the point $\boldsymbol{C}$ within the camera coordinate system R_C, to a pixel represented by a 2D point $\boldsymbol{m}$ within the 2D image frame R_I. This transformation entails the use of the camera's focal length f and a scale factor s to achieve accurate mapping. It can be expressed as follows:

$$s \cdot \begin{bmatrix} x_{\boldsymbol{i}} \\ y_{\boldsymbol{i}} \\ 1 \end{bmatrix} = \begin{bmatrix} f & 0 & 0 & 0 \\ 0 & f & 0 & 0 \\ 0 & 0 & 1 & 0 \end{bmatrix} \cdot \begin{bmatrix} X_{\boldsymbol{C}} \\ Y_{\boldsymbol{C}} \\ Z_{\boldsymbol{C}} \\ 1 \end{bmatrix} \tag{3.4}$$

The significance of this transformation is elucidated with reference to Figure 3.1, where the point $\boldsymbol{m}$ is observed as the 2D reflection of 3D point $\boldsymbol{M}$ located in the 3D world reference frame R_W after passing through the camera coordinate system R_C and subsequently onto the image frame R_I.

The determination of the homogeneous 2D coordinates $\hat{\boldsymbol{x}}_{\boldsymbol{s}} = [x_s, y_s, 1]^{\mathrm{T}}$ of the projection point $\boldsymbol{m}$ in the sensor frame R_S is the responsibility of the **third transformation**. This transformation takes into account various camera characteristics, including:

- Skew Angle: The angle between the horizontal and vertical axes of the sensor. In this case, it is assumed to be equal to 90°;
- Optical Center Position: The position of the optical center, which serves as the reference point for the projection;
- Pixel Physical Size: The physical size of the pixel in both the horizontal and vertical directions. This parameter affects the overall scale and resolution of the projected image.

These various internal camera characteristics can be integrated into a 3×4 projection matrix denoted as $\boldsymbol{K}$:

$$\boldsymbol{K} = \begin{bmatrix} f_{\boldsymbol{x}} & \boldsymbol{d} & c_{\boldsymbol{x}} & \boldsymbol{0} \\ \boldsymbol{0} & f_{\boldsymbol{y}} & c_{\boldsymbol{y}} & \boldsymbol{0} \\ \boldsymbol{0} & \boldsymbol{0} & \boldsymbol{1} & \boldsymbol{0} \end{bmatrix} \tag{3.5}$$

This projection matrix is determined by five intrinsic parameters associated with the calibrated camera: the horizontal $f_{\boldsymbol{x}}$ and vertical $f_{\boldsymbol{y}}$ focal lengths in pixels, as well as the position $(c_{\boldsymbol{x}}, c_{\boldsymbol{y}})$ in pixels of the optical center within the entire image plane. Additionally,

it includes a skew coefficient d, which is non-zero when the image axes are not perfectly perpendicular. We refer to this matrix as the camera *Intrinsic Matrix*. And it contribute to the accurate representation of the projected point in the sensor frame R_S.

The complete projection matrix $\boldsymbol{M}$, which characterizes a camera, is thus formed by combining an extrinsic parameter matrix $\boldsymbol{T}$ and an intrinsic parameter matrix $\boldsymbol{K}$, formulated as follows:

$$s \cdot \mathrm{x_s} = \left[\boldsymbol{K}\right] \cdot \left[\boldsymbol{T}\right] \cdot \mathrm{X_W} = \left[\boldsymbol{M}\right] \cdot \mathrm{X_W} \tag{3.6}$$

From the three transformations mentioned above, it becomes evident that camera calibration aims to estimate intrinsic parameters and extrinsic parameters, represent those of its projection matrix $\boldsymbol{M}$.

3.2. Laser Line Model

A line in 3-space is determined by either joining two points or the intersection of two planes. Such lines possess four degrees of freedom. An effective approach to understanding these degrees of freedom is to envision a line as characterized by its intersection with two mutually perpendicular planes, as depicted in Figure 3.3. As evident in the image, a line may be specified by its points of intersection with two orthogonal planes. And on each plane, the point of intersection is defined by two parameters, resulting in a collective total of four degrees of freedom associated with the line.

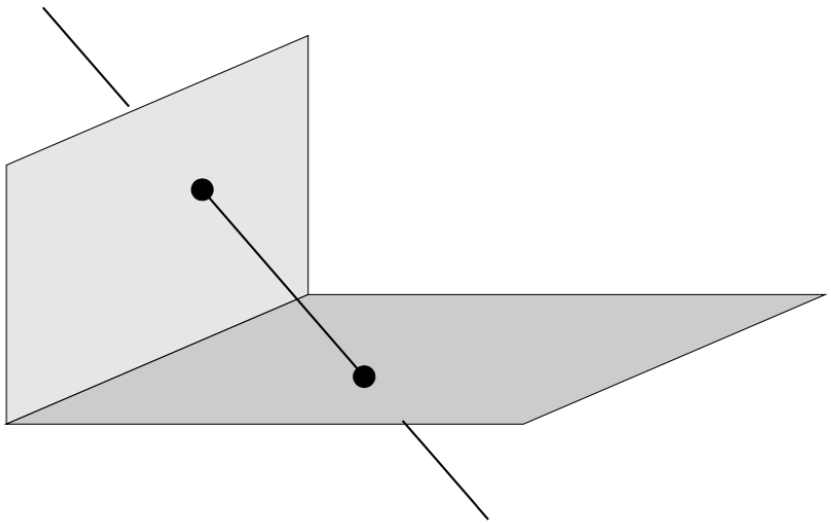

Figure 3.3: Defining A Line in Three-Dimensional Space [1].

Representing the line in 3-space can be challenging because an object with 4 degrees of freedom would naturally be represented as a homogeneous 5-vector. However, using a homogeneous 5-vector alongside the 4-vectors representing points and planes in mathematical expressions can be cumbersome. To address this issue, various line representations have been proposed, each with its own level of mathematical complexity.

3.2.1. Plücker Matrices Representation

This article utilizes the Plücker matrix representation, which offers several ways to define the line: through the connection of two points, a dual version where the line arises from the intersection of two planes, and a mapping between these two definitions. It also facilitates the computation of join and incidence relations, such as determining the point where a line intersects a plane.

In the Plücker matrix representation, a line is symbolized by a 4×4 skew-symmetric homogeneous matrix. Specifically, the line that connects two points, $\mathbf{A}$ and $\mathbf{B}$, is expressed by the matrix $\boldsymbol{L}$, consisting of elements:

$$l_{ij} = A_i B_j - B_i A_j \tag{3.7}$$

Alternatively, in vector notation equivalently can be expressed as:

$$\boldsymbol{L} = \mathbf{A}\mathbf{B}^T - \mathbf{B}\mathbf{A}^T \tag{3.8}$$

Let's break down a few key properties of $\boldsymbol{L}$:

- The matrix $\boldsymbol{L}$ possesses a rank of 2. Its 2-dimensional null-space is generated by a group of planes that share the line as their common axis. In mathematical terms, this can be expressed as $\mathrm{LW}^{\mathrm{T}} = 0$, where 0 represents a 4×2 null-matrix;
- The representation has the necessary 4 degrees of freedom to define a line. This can be explained as follows: The skew-symmetric matrix has 6 independent non-zero elements, but only 5 of their ratios are meaningful. Additionally, due to `det L = 0`, these elements satisfy a quadratic constraint. Consequently, the effective number of degrees of freedom is 4;
- The relation 3.8 is the generalization to 4-space of the vector product formula `l = x × y` of IP^2 which is the projective space. It defines a line `l` based on two points `x` and `y`, all represented by 3-vectors;

- During the point transformation $X' = HX$, the matrix undergoes a transformation as well, changing into $L' = HLH^T$. In essence, this matrix can be classified as a valency-2 tensor;
- The matrix $\boldsymbol{L}$ is independent of the points $\mathbf{A}$, $\mathbf{B}$ used to define it. This independence stems from the fact that even if a different point $\mathbf{C}$ along the same line is employed, denoted as $\mathbf{C} = \mathbf{A} + \mu\mathbf{B}$, the resulting matrix follows this pattern:

$$\begin{aligned}\hat{\boldsymbol{L}} = \mathbf{A}\mathbf{C}^T - \mathbf{C}\mathbf{A}^T = \mathbf{A}(\mathbf{A}^T + \mu\mathbf{B}^T) - (\mathbf{A} + \mu\mathbf{B})\mathbf{A}^T = \\ \mathbf{A}\mathbf{B}^T - \mathbf{B}\mathbf{A}^T = \boldsymbol{L}\end{aligned} \tag{3.9}$$

Based on the description above, the X-axis is represented as:

$$\boldsymbol{L} = \begin{bmatrix} 0 \\ 0 \\ 0 \\ 1 \end{bmatrix} \begin{bmatrix} 1 & 0 & 0 & 0 \end{bmatrix} - \begin{bmatrix} 1 \\ 0 \\ 0 \\ 0 \end{bmatrix} \begin{bmatrix} 0 & 0 & 0 & 1 \end{bmatrix} = \begin{bmatrix} 0 & 0 & 0 & -1 \\ 0 & 0 & 0 & 0 \\ 0 & 0 & 0 & 0 \\ 1 & 0 & 0 & 0 \end{bmatrix}$$

Where the points $\mathbf{A}$ and $\mathbf{B}$ are the origin and ideal point in the X-direction respectively.

3.2.2. Dual Plücker Representation

A dual Plücker representation, denoted as $\boldsymbol{L}^*$, is obtained for a line formed by the intersection of two planes, $\mathbf{P}$ and $\mathbf{Q}$:

$$\boldsymbol{L}^* = \mathbf{P}\mathbf{Q}^T - \mathbf{Q}\mathbf{P}^T \tag{3.10}$$

It possesses analogous properties to L. When subjected to the point transformation $X' = HX$, the matrix $\boldsymbol{L}^*$ transforms as $\boldsymbol{L}^* = H^{-T}\mathbf{L}H^{-1}$. The matrix $\boldsymbol{L}^*$ can be derived directly from $\boldsymbol{L}$ using a straightforward rewriting rule:

$$l_{12} : l_{13} : l_{14} : l_{23} : l_{42} : l_{34} = {l_{34}}^* : {l_{42}}^* : {l_{23}}^* : {l_{14}}^* : {l_{13}}^* : {l_{12}}^* \tag{3.11}$$

The correspondence rule is quite straightforward: the indices of the dual and original components always encompass all the numbers {1, 2, 3, 4}. Therefore, if the original is represented by `ij`, then the dual is formed by those numbers from {1, 2, 3, 4} that are not in `ij`. For instance, 12 is transformed to 34.

Join and incidence properties are very elegantly represented in this notation. The plane formed by joining the point $\mathbf{X}$ and the line $\boldsymbol{L}$ is defined as:

$$\boldsymbol{\pi} = \mathbf{X}\boldsymbol{L}^* \tag{3.12}$$

The condition $\mathbf{X}\boldsymbol{L}^* = \mathbf{0}$ holds if and only if point $\mathbf{X}$ lies on line $\boldsymbol{L}$. And, the point defined by the intersection of the line $\boldsymbol{L}$ with the plane $\boldsymbol{\pi}$ is:

$$\mathbf{X} = \boldsymbol{\pi}\boldsymbol{L} \tag{3.13}$$

The condition $\boldsymbol{\pi}\boldsymbol{L} = \mathbf{0}$ holds if, and only if, line $\boldsymbol{L}$ lies on plane $\boldsymbol{\pi}$. The properties of two (or more) lines, denoted as L_1, L_2, and so on, can be derived from the null-space of the matrix $\boldsymbol{N}$, defined as $\boldsymbol{N} = [L_1, L_2, ...]$. For instance, if these lines lie in the same plane, the transpose of $\boldsymbol{N}$, $\boldsymbol{N}^{\mathrm{T}}$, will have a 1-dimensional null-space representing the plane $\boldsymbol{\pi}$ formed by these lines.

Based on the previous explanation, let's consider an example. The intersection of the X-axis with the plane $\mathbf{X} = 1$ is given by $\mathrm{X} = \boldsymbol{\pi}\boldsymbol{L}$ as:

$$\mathbf{X} = \begin{bmatrix} 0 & 0 & 0 & -1 \\ 0 & 0 & 0 & 0 \\ 0 & 0 & 0 & 0 \\ 1 & 0 & 0 & 0 \end{bmatrix} \begin{bmatrix} 1 \\ 0 \\ 0 \\ -1 \end{bmatrix} = \begin{bmatrix} 1 \\ 0 \\ 0 \\ 1 \end{bmatrix}$$

which is the inhomogeneous point $(\mathrm{X}, \mathrm{Y}, \mathrm{Z})^{\mathrm{T}} = (1, 0, 0)^{\mathrm{T}}$.

3.2.3. Plücker Line Coordinates

The Plücker line coordinates comprise the six non-zero elements found within the 4x4 skew-symmetric Plücker matrix [3.8], which are as follows:

$$\mathcal{L} = \left\{ l_{12}, l_{13}, l_{14}, l_{23}, l_{42}, l_{34} \right\} \tag{3.14}$$

This forms a homogeneous 6-vector, making it an element within IP^5. It can be deduced from the evaluation of `det L = 0` that these coordinates adhere to the equation:

$$l_{12}l_{34} + l_{13}l_{42} + l_{14}l_{23} = \mathbf{0} \tag{3.15}$$

A 6-vector $\mathcal{L}$ represents a line in 3-space only when it meets the condition satisfies above equation. Geometrically, this constraint signifies that the lines in IP^3 define a surface within IP^5, referred to as the *Klein quadric*, a quadric because the terms of above equation are quadratic in the Plücker line coordinates.

Let's consider two lines, $\mathcal{L}$ and $\hat{\mathcal{L}}$, formed by joining points **A**, **B**, and , , respectively. These two lines intersect if and only if all four points are coplanar. A necessary and sufficient condition for this is that `det[A,B,`$\hat{A}$`,`$\hat{B}$`] = 0`. It can be shown that the determinant expands as:

$$\begin{aligned} \texttt{det[A,B,}\hat{A}\texttt{,}\hat{B}\texttt{]} = l_{12}\hat{l_{34}} + \hat{l_{12}}l_{34} + l_{13}\hat{l_{42}} + l_{14}\hat{l_{23}} + \hat{l_{14}}l_{23} \\ = (\mathcal{L}|\hat{\mathcal{L}}) \end{aligned} \tag{3.16}$$

Given that the Plücker coordinates are independent of the particular points used to define them, the bilinear product $(\mathcal{L} \mid \hat{\mathcal{L}})$ is independent of the points used in the derivation and only depends on the lines $\mathcal{L}$ and $\hat{\mathcal{L}}$. This leads to a crucial conclusion: Two lines, $\mathcal{L}$ and $\hat{\mathcal{L}}$, are coplanar (and consequently intersect) if and only if $(\mathcal{L} \mid \hat{\mathcal{L}})$ equals zero.

This conclusion appears in several valuable formula: A 6-vector $\mathcal{L}$ accurately represents a line in IP^3 only when $(\mathcal{L} \mid \hat{\mathcal{L}}) = 0$. This is essentially reiterating the Klein quadric constraint [3.15] mentioned earlier. And suppose two lines $\mathcal{L}$, $\hat{\mathcal{L}}$ are the intersections of the planes **P**, **Q** and $\hat{P}$, $\hat{Q}$ respectively. Then:

$$(\mathcal{L}|\hat{\mathcal{L}}) = \texttt{det}[\mathbf{P}, \mathbf{Q}, \hat{P}, \hat{Q}] \tag{3.17}$$

and again the lines intersect if and only if $(\mathcal{L} \mid \hat{\mathcal{L}}) = 0$. Furthermore, if $\mathcal{L}$ represents the intersection of two planes **P** and **Q**, and $\hat{\mathcal{L}}$ represents the join of two points **A** and **B**, then the following relationship holds:

$$(\mathcal{L}|\hat{\mathcal{L}}) = (\mathbf{P}^T\mathbf{A})(\mathbf{Q}^T\mathbf{B}) - (\mathbf{Q}^T\mathbf{A})(\mathbf{P}^T\mathbf{B}) \tag{3.18}$$

It is crucial to establish a common reference frame between the camera and laser line system in this experiment. This involves transforming points and lines from one system to another. Plücker matrix representation for lines facilitates this transformation efficiently.

3.3. Taking Distortion into Account

The line modeling described above is integrated with equation 3.3 of the Section 3.1 to accomplish the extrinsic calibration among various sensors. This process is elucidated extensively in the subsequent chapter, Chapter 4. Additionally, imperfections in the optical system, such as irregularities in the shape and alignment of the camera lenses, can lead to distortions in the projected image. These distortions cause light rays to deviate from their expected positions, resulting in a positional discrepancy between multiple images of light rays and an ideal model(refer to Figure 3.1). To create a comprehensive camera model, it is necessary to introduce three primary types of distortions that have the most significant impact, as illustrated in Figure 3.4. These distortions are radial, decentering, and prismatic distortions, and they arise from issues related to curvature, lens parallelism and coaxiality of the optical axes.

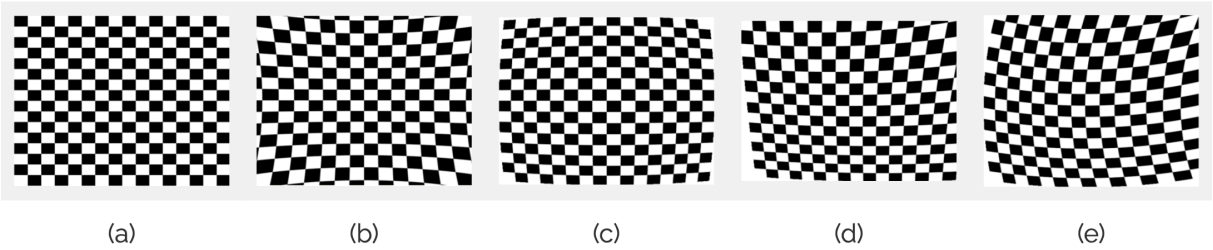

Figure 3.4: (a) Ideal Image and Effects of (b) Positive Radial, (c) Negative Radial, (d) Decentering and (e) Prismatic Distortions. [34]

Inaccurate camera calibration frequently results in measurement distortions in both displacements and deformations. Thus, the question arises: How can we prevent these camera calibration errors? To guarantee accurate calibration, it may be advisable to capture images of well-defined rigid body motions that include lens distortion (translation) of known amplitude. Subsequently, we can validate the displacement measurements by comparing them with the distorted image data to ensure consistency. Simultaneously, the effectiveness of distortion reduction is greatly enhanced by employing an algorithm characterized by strong stability, robustness, and high precision.

4 | Experimental Setup and Evaluation

4.1. Real Calibration Dataset Collection

In this experiment, a `Basler acA 2040-90um USB 3.0` camera and a red laser source with a wavelength of `650nm` were applied to do the calibration setup work. The Basler ace camera is a high-speed camera with a `2048 x 2048` pixel resolution and a maximum frame rate of `90` frames per second. And the camera is equipped with a `C-mount` lens mount and is capable of capturing high-quality images with low noise and high sensitivity.

To acquire accurate and meaningful data, it is essential to ensure the calibration target, specifically the checkerboard image, possesses a high degree of smoothness, uniformity and regularity. This minimizes the adverse effects of distortion. In this regard, we employed a computer monitor as the flat support for the checkerboard image, which yielded favorable outcomes. For a comprehensive overview of the experimental setup described above, please refer to Figure 3.2.

With the help of these experimental devices, real image data is collected and organized in a structure. The detail of this structure will be described in-depth in the subsequent section. Figure 4.2 serves as a intuitive visual reference, demonstrating a practical utilization of camera extrinsic parameters from that structure which including the rotation matrix and translation vector.

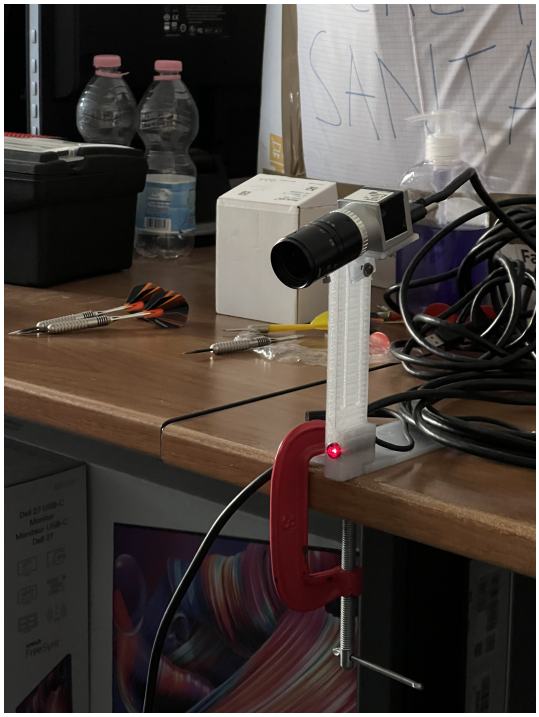

(a) The Camera and The Laser Line Sensor

(b) The Checkerboard Image on The Monitor

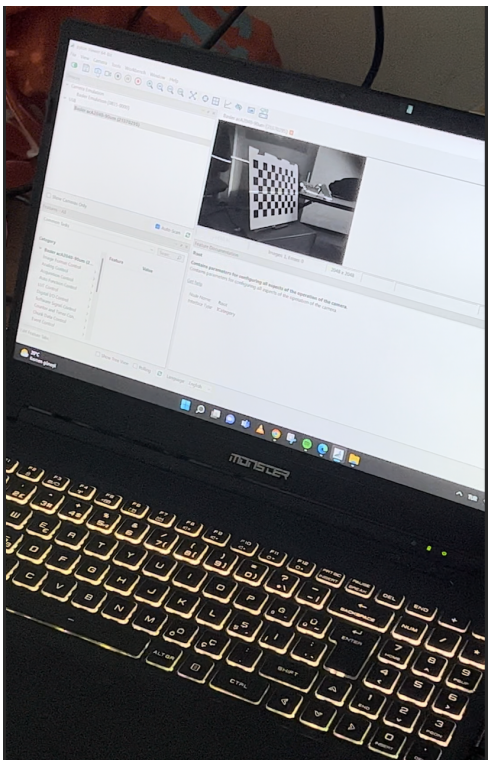

(c) Acquisition of Real Image Data

Figure 4.1: Experimental Setup.

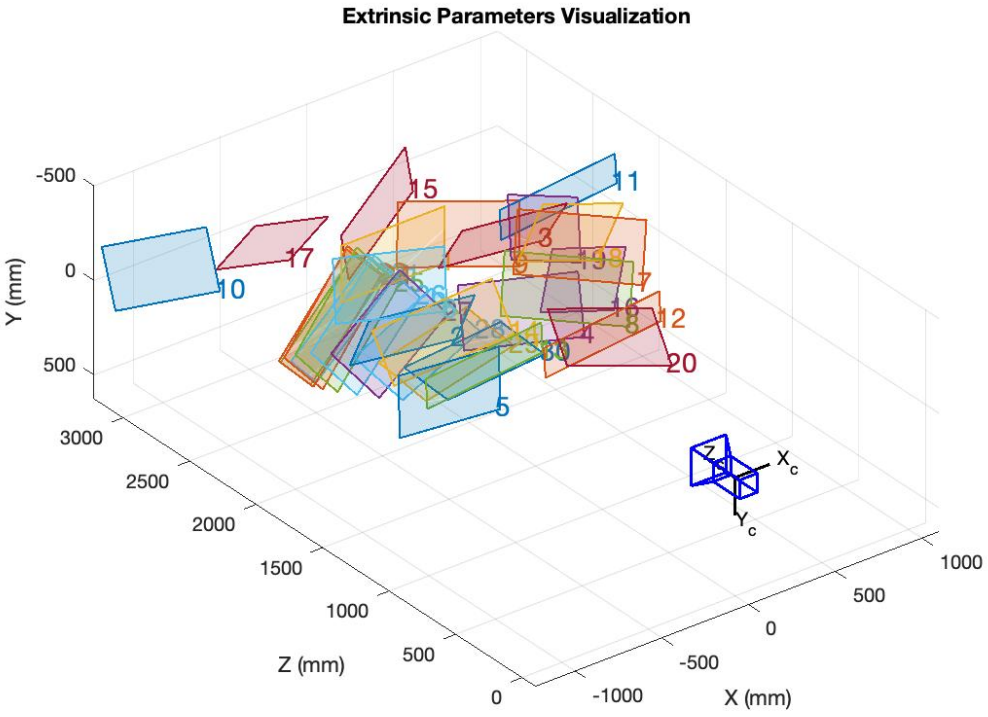

Figure 4.2: Visual Representation Based on Extrinsic Parameters.

4.1.1. Re-projection Errors Related to This Experiment

The re-projection errors are a global measure of calibration error and the difference between the points detected in the image and points reprojected back onto the image using the parameters that just calculated and stored in a data structure. For a clearer comprehension, kindly consult Figure 4.3. In essence, these errors represent the discrepancies between the observed positions of known calibration points in the image and their corresponding positions in the real world.

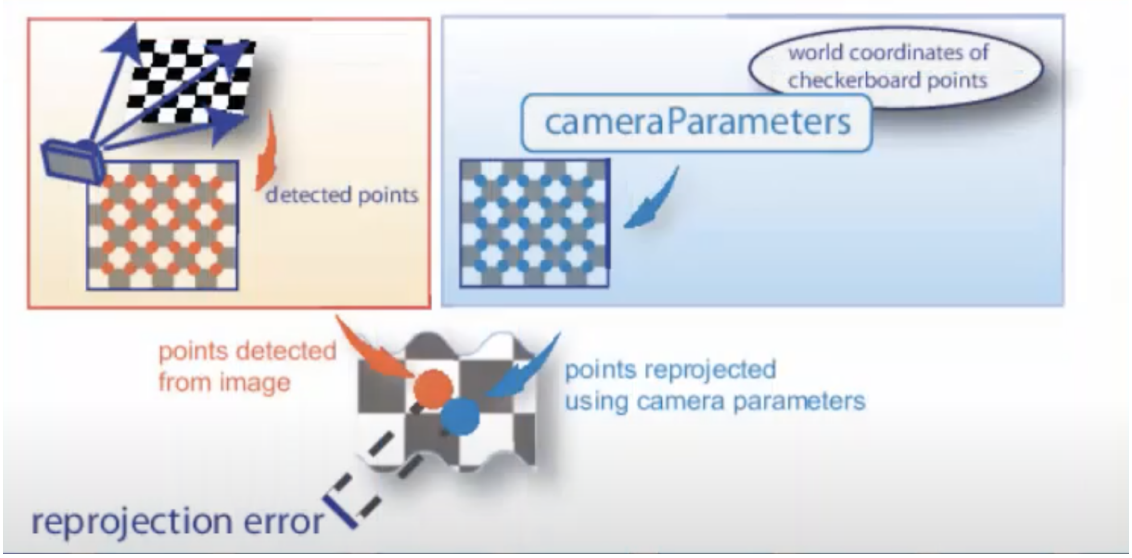

Figure 4.3: Re-projection Error.

The calibration results can be evaluated by visualizing reproduction error. Figure 4.4 shows it related to this experiment. The objective is to identify the best-fitting transformation that minimizes these errors. By comparing the projected 2D points (from 3D world coordinates) with the actual 2D image points, the calibration algorithm adjusts the extrinsic parameters until the re-projection errors are minimized. This ensures that the pose of the camera in the world coordinates is accurately determined.

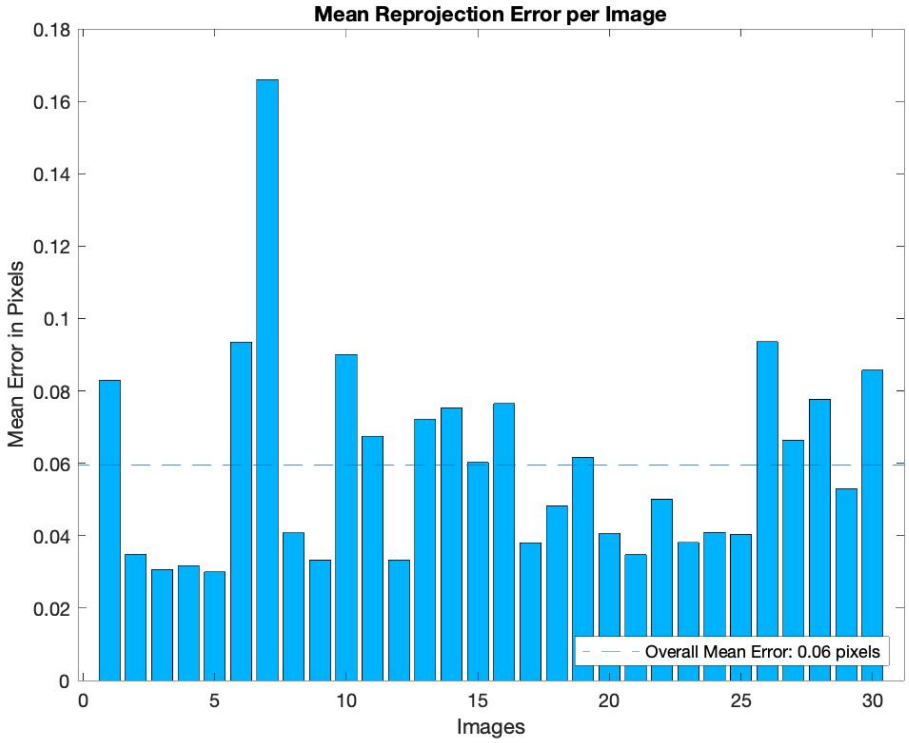

Figure 4.4: Visualization of The Re-projection Errors.

4.2. Software Configuration

The objective of this experiment is to determine the plane of the laser line relative to the position/orientation of the camera, essentially performing extrinsic calibration for the camera and the laser. To achieve this, we intersect the laser line with a series of checkerboards of known dimensions, thus achieving the dual purpose of calibrating the camera optics and determining the plane of the laser line. In an ideal scenario devoid of noise and acquisition errors, only two images with the checkerboards in different positions would suffice to solve the problem (with geometric precision: "provided that the two planes of the checkerboards and the laser line do not belong to the same plane bundle"). However, in a real-world context, various sources of error and noise exist in the acquisition process that need to be minimized.

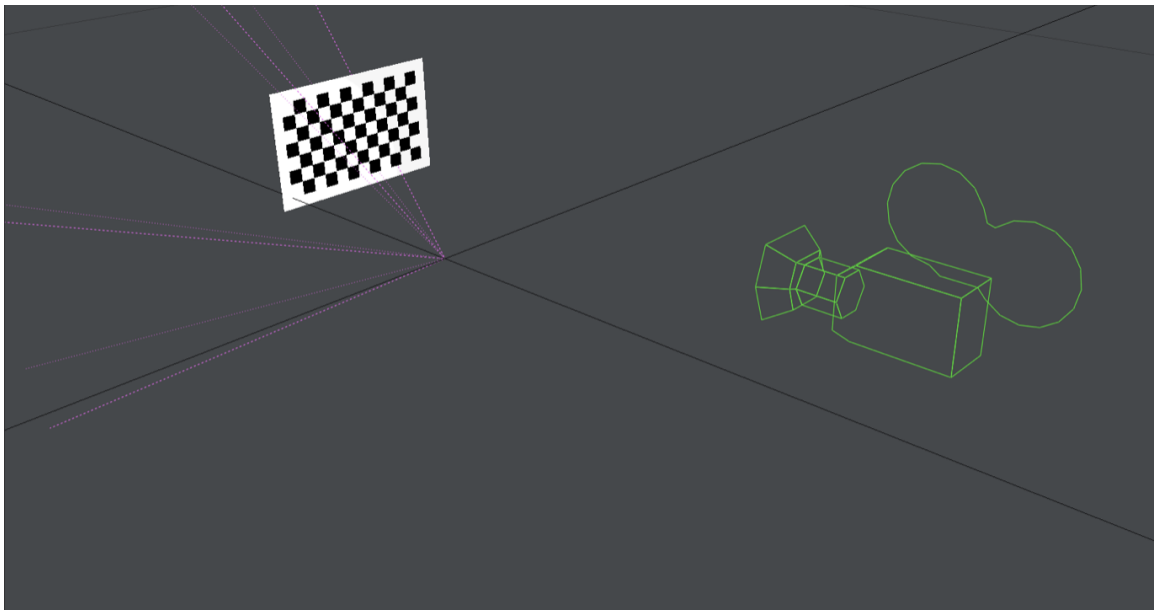

Figure 4.5: Three-Dimensional Simulation of The Experiment Setup.

4.2.1. Commence with Camera Calibration

In the folder *"cameraIntrinsic"*, there is a series of images of the checkerboard (without the laser line) captured in different positions by the experimental setup in Section 4.1. Then Using the *MATLAB Computer Vision Toolbox* app for camera intrinsic parameter calibration, to obtain and store the calibration parameters in a structure called ***cameraParams***. You can directly load these parameters from the *"intrinsic.mat"* file located in the same folder. This structure contains the parameters that describe the camera acquisition system, including the radial distortion, the focal length, the skew coefficient and the optical center, also known as the principal point (which may not always coincide precisely with the image center). It is worth mentioning that all measurements are in pixels due to the absence of "pixel size" information, which represents the physical dimensions of each individual pixel on the camera sensor. Consequently, the parameters such as focal length and principal point are all quantified in pixels. In reality, as detailed in Section 3.1, the intrinsic parameters $(f_{\boldsymbol{x}}, f_{\boldsymbol{y}})$, which represent the focal length in pixels, and $(c_{\boldsymbol{x}}, c_{\boldsymbol{y}})$, denoting the optical center/principal point in pixels. They compose the intrinsic matrix $\boldsymbol{K}$[3.5], are both specified in pixels. And if F is defined as the focal length in world units, which is typically expressed in millimeters, and the size of the pixel in world units is described as $(p_{\boldsymbol{x}}, p_{\boldsymbol{y}})$. Then the relationship between these parameters can be formulated as follows: $f_{\boldsymbol{x}} = F/p_{\boldsymbol{x}}$, $f_{\boldsymbol{y}} = F/p_{\boldsymbol{y}}$.

On the other hand, the translation vectors and rotation matrices, are responsible for

reprojecting each checkerboard accurately into the reference system of the camera for every frame, considering the structure of the checkerboard(in this case, the square dimensions are provided in millimeters). To illustrate, if we take the checkerboard defined in the `WorldPoints` matrix within ***cameraParams***, the coordinates of the first three corners (linked to the first three squares of the checkerboard) are as follows:

$$p_1 = \begin{bmatrix} x_1 \\ y_1 \\ z_1 \end{bmatrix} = \begin{bmatrix} 0 \\ 0 \\ 0 \end{bmatrix}, p_2 = \begin{bmatrix} 0 \\ 60 \\ 0 \end{bmatrix}, p_3 = \begin{bmatrix} 0 \\ 120 \\ 0 \end{bmatrix} \tag{4.1}$$

To obtain the spatial coordinates of these points after the rotation-translation, which brings the checkerboards from having their origin coinciding with the reference system origin of the camera to the coordinates they had when they were acquired, it is necessary to apply the transformation using the rotation matrices and the indicated translation vectors. This operation is performed in 3D space:

$$P_n = \boldsymbol{R} \cdot p_n + \boldsymbol{t} \tag{4.2}$$

In the meanwhile, you can refer to Figure 4.6,

Figure 4.6: The reference system is transferred using extrinsic parameters.

Subsequently, if you intended to obtain the (homogeneous) coordinates of the corner points on the image plane, with the exclusion of re-projection errors, you would execute a multiplication of the 3D points of the camera coordinates which is obtained by the above equation in the by the intrinsic matrix $\boldsymbol{K}$. To view the entire flowchart illustrating the transformation of coordinate systems via intrinsic and extrinsic parameters, please consult Figure 4.7.

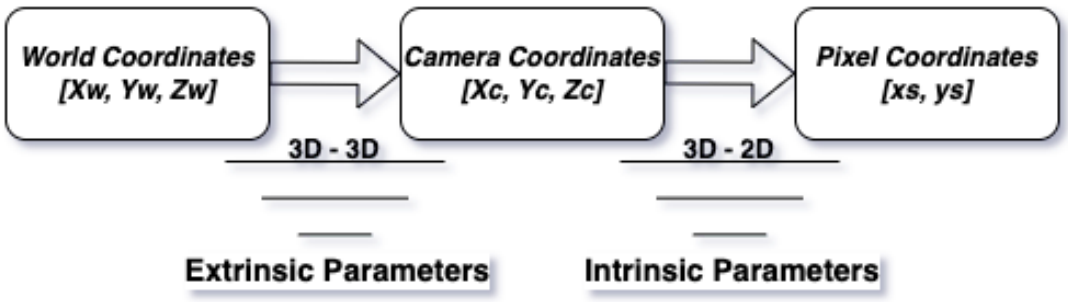

Figure 4.7: The Transformation Flow Chart.

In our project, we need to know the 3D coordinates P_n of the checkerboard corners in the camera coordinate system R_C. This information will enable us to determine the positions of the checkerboard planes in space within the reference system of the camera and ultimately facilitating the determine of their spatial intersection with the laser line plane.

4.2.2. Determining The Position of The Checkerboards in Space "Cut" by The Laser Line

We are now calculating the spatial position of the checkerboards that have been intersected by the laser line. While we could certainly use the same checkerboards that were employed during the previous phase which is in Section 4.2.1, but in this case, we use a reduced number of boards with the blue laser line positioned above them. These checkerboards can be found in the *"calibrationCameraLaserImages"* folder.

The process described above is accomplished through Function 4.1, which is responsible for deriving the rotation matrix and translation vector for these checkerboards based on the checkerboard image, the intrinsic parameters of the camera, and the dimensions of the squares in millimeters. The returned parameter, `outputTarget`, serves the sole purpose of verification, as it applies a marker to each corner of the checkerboard. This marker aids in validating the accuracy of the estimated rotation matrix and translation vector.

```
function [rotationMatrix, translationVector, outputTarget, points3D,
    HorizPlane] = findCheckerboard3DPosition(target, cameraParams,
    squareSizeInMillimeters)
```

Listing 4.1: Function findCheckerboard3DPosition

4.2.3. Determining The Position of The Intersection Line Between The Laser Line and The Checkerboard Plane

Firstly, the calculation of the blue laser line in the images (checkerboard planes) is performed using these two functions,

```
1 function [Y,X,im] = bluePointExtraction(inputPar)
2 function param = lineExtraction(inputPar)
```

Listing 4.2: Function bluePointExtraction & lineExtraction

where `1` takes as input an image (or the filename of an image) and identifies the blue pixels, returning their coordinates in arrays of X and Y. And `2` also receives an image, or the filename of an image, as input and calculates the parameters a, b, c of the line equation $ax + by + c = 0$ in the image plane. It performing by calling the function `bluePointExtraction` to extract the three line coefficients from blue pixels in an image, coefficients are in the pixel format.

Afterward, we can determine the spatial position of the intersection line between the checkerboard plane and the laser line. For this purpose, it is necessary to define a third plane, that pass through the center of the camera (global reference system) and the spatial intersection line between the laser line and the checkerboard plane. This plane essentially represents the spatial re-projection (inverse projection) in three-dimensional space of the line segment that, within the image plane, corresponds to the projection of the intersection line between the checkerboard and the laser line. For improved comprehension, please refer to Figure 4.8.

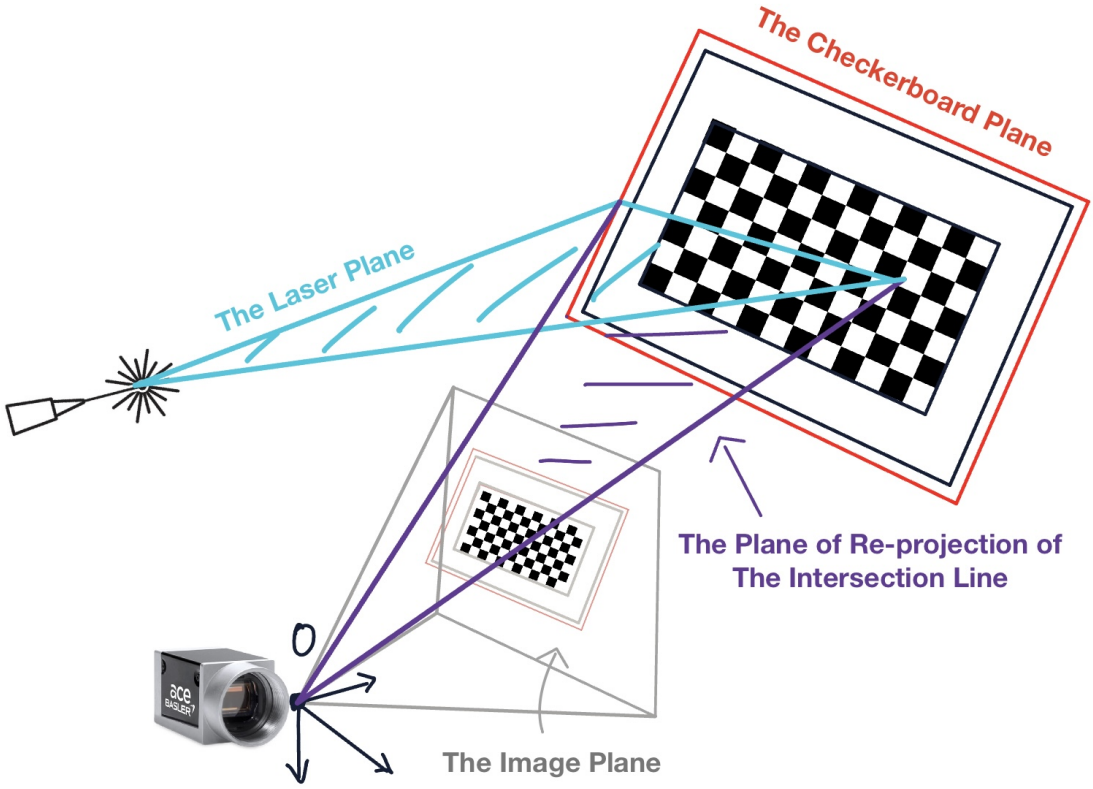

Figure 4.8: 3D Spatial Representation of The Experimental Setup Model and The Inter-relation Between Various Planes.

The formulation of the intersection line, which serves as the axis of the bundle formed by the three planes (checkerboard, laser line, and re-projection of line segment), is accomplished using Plücker notation with the below function,

```
function [L, H, P] = pluckerLineFromCheckerboarImagePlusLaser(
    checkerboardImage, checherboardImagePlusLaser, cameraParams,
    squareSizeInMillimeters, ReferenceRotation,ReferenceTranslation)
```

Listing 4.3: Function pluckerLineFromCheckerboarImagePlusLaser

Where the 3x4 projection matrix of the camera was constructed in, denoted as P_{cam}. It assuming the camera in the origin of the reference system with optical axis along the z axis. And given a 3D point in homogeneous coordinates, it returns its 2D homogeneous coordinates on the image plane. For the another projection matrix P which is as the output parameter in this function, it is obtained by incorporating the intrinsic matrix of the camera along with the rotation matrix and translation vector(`rotationMatrix`,

`translationVector`), which are determined based on the assumption that the checkerboard in the current frame serves as the general reference system. It involves using the Function 4.1. This is a necessary step because in the project a series of measurements had to be obtained with respect to a specific reference system, as shown in Figure 4.9. Therefore, all measurements are transformed into this reference system, which is determined by the reference system of the first checkerboard coplanar with the specific reference system. Another output parameter, *H*, is the 4x4 homography matrix that projects 3D points from the camera reference frame into the world reference frame. Its component elements, `rotationMatrix`, and `translationVector`, are obtained from the current actual checkerboard image. In contrast, `ReferenceRotation` and `ReferenceTranslation` represent the rotation and translation of the camera with respect to a global reference system, as represented by the cartesian axis on the first checkerboard image. These two input parameters are used to construct the 3D homography matrix, *Href*, which is also a 4x4 matrix responsible for rigidly transforming points in 3D space from camera coordinates *O* to coordinates in the reference plane *O'*.

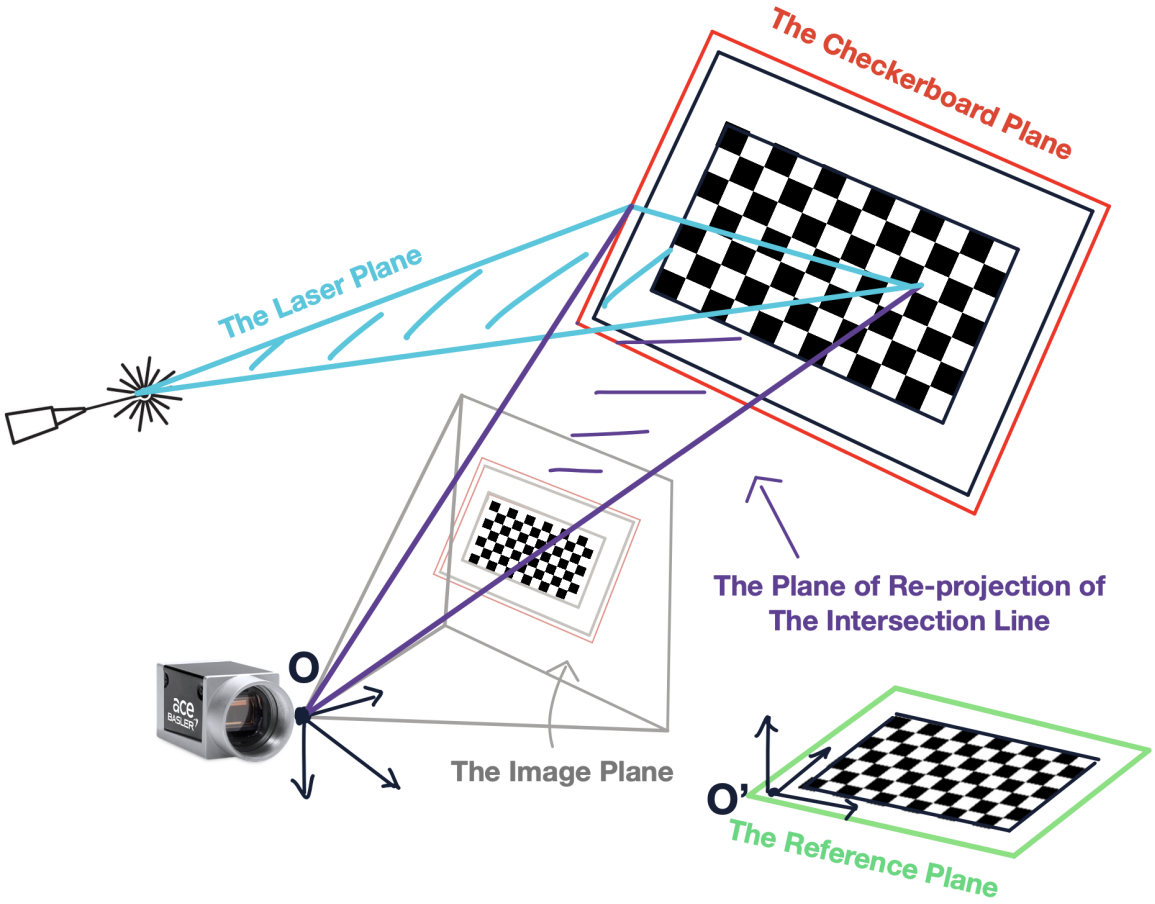

Figure 4.9: 3D Spatial Representation and The Reference Plane.

The first *if* conditional statement in Function 4.3 serves to confirm the two conditions related to the utilization of distinct checkerboards as previously discussed:

- In the first condition, a reference frame was defined using .e.g the first image of the checkerboard. In order to obtain the 3D Plücker line relative to that reference system. This involves a transformation process. Given the equation $Plane \times X = 0$, which can be expressed as $Plane \times H^{-1} \times H \times X = 0$, we can see that for transformed points $H \times X$, the plane transforms accordingly: $newPlane = Plane \times inv(H)$, which can be rewritten as $newPlane' = inv(H)' \times Plane'$;
- In the second condition, the current actual plane assumes the role of the reference since the reference frame has not been defined. This condition happens during the initial steps of a calibration process. And in this condition, any 3D line being worked with is associated with or linked to this actual plane. Essentially, it is as if this plane serves as the reference for that line. This suggests that, within the reference frame

defined by this plane, the z-coordinates of points on the 3D line will consistently have a value of zero.

As depicted in Figure 4.9, the plane passing through a line in the image (placed in the 3D framework) and the optical center of the camera, that is the re-projection plane, then the re-projection of a line from an image into the space defining this plane. The re-projection plane is determined by straightforwardly pre-multiplying the equation of the laser line in the image plane by the transpose of the projection matrix which is the P: $line \times x = 0 \rightarrow line \times (P \times X) = 0 \rightarrow (line \times P) \times X = 0 \rightarrow X' \times P' \times line' = 0$. And the re-projection is performed with the assumption that the coordinate system is centered at the camera's center, and in the Function 4.3, it is expressed as follows:

```
reprojectedPlaneFromLaserLine = Pcam' * line;
```

Where the *line* is obtained from Function 4.2 (*lineExtraction*). Additionally, in the first *if* conditional statement, it is worth noting that both conditions invoke the following Function 4.4,

```
1 function [L_matrix, L, L_matrix_dual] = PluckerLineFromTwoPlanes(A, B)
```

Listing 4.4: Function PluckerLineFromTwoPlanes

The function takes two input parameters, A and B, which are represented as two 4-element column vectors containing the plane parameters a, b, c, and d from the equation $ax + by + cz + d = 0$. According to the principles outlined in Section 3.2, the function returns the 4x4 matrix `L_matrix`, its dual `L_matrix_dual`, and a 6-element column vector `L`$(l_{12} : l_{13} : l_{14} : l_{23} : l_{42} : l_{34})$, which represents the line. However, it is essential to note that all transpositions are consistently applied to align with the notation in Section 3.2, which is inverted compared to the convention of MATLAB convention. Therefore, in practical MATLAB applications, the line is represented as:

```
L = [L_matrix(1,4) L_matrix(4,2) L_matrix(3,4) L_matrix(2,3)...
L_matrix(1,3) L_matrix(1,2)];
```

In the case of calling Function 4.4 for the first checkerboard, the origin of that checkerboard becomes the origin of the entire reference system. The plane of that checkerboard becomes the plane:

```
checkerboardPlaneEquation = [0 0 1 0]';
```

Represents the checkerboard plane located at the origin. The 3D homography matrix then becomes the one that rigidly transforms everything from the camera reference system to the "first checkerboard" reference system. So:

```
H = [rotationMatrix' translationVector'; [0 0 0 1]];
```

When the parameter `ReferenceRotation` is empty, it signifies that the reference frame is undefined. This typically occurs during the initial frame of the calibration process when the first checkerboard plane intersects with the laser plane. During this phase, the re-projection plane is represented by `"H'*reprojectedPlaneFromLaserLine"` and `"checkerboardPlaneEquation"` from which:

```
[ ~, L, ~] = PluckerLineFromTwoPlanes(H' * reprojectedPlaneFromLaserLine,
checkerboardPlaneEquation);
```

In Function 4.4, and it constitutes the second condition within the first "*if*" conditional statement. For the subsequent acquisitions where the `ReferenceRotation` matrix and `ReferenceTranslation` vector related to the reference frame are already defined, it is possible to define the transformation:

```
Href = [ReferenceRotation ReferenceTranslation; [0 0 0 1]];
```

And consequently refer directly to the new reference system:

```
[ ~, L,~] = PluckerLineFromTwoPlanes(Href' * reprojectedPlaneFromLaserLine,
Href' * (H' \ checkerboardPlaneEquation));
```

Where the second argument specifies that for each subsequent checkerboard plane (which is always defined as `[0 0 1 0]`), the transformation first takes it into the the reference plane of the camera and then into the reference system of the first checkerboard.

4.2.4. Determining The Laser Plane

The script *"extractionLaserPlane.m"* loads a series of images from the *"calibrationSystem"* folder and, for each image, determines the line [`L_matrix`, `L`, `L_matrix_dual`] according to the Plücker notation in the three formulations mentioned above, thereby creating three tensors `[L(:,cursor), H(:,:,cursor), P(:,:,cursor)]` with the following Function 4.3 call:

```
[ L(:,cursor), H(:,:,cursor), P(:,:,cursor)]=
pluckerLineFromCheckerboarImagePlusLaser(image, image, cameraParams, 60,
H(1:3,1:3,1), H(1:3,4,1) );
```

Then, the Function 4.5 operates directly on the first tensor `L(:,cursor)` based on the `L_matrix`.

```
function [laserPlane] = laserPlaneFromMultiplePluckerLines(LBlock)
```

Listing 4.5: Function laserPlaneFromMultiplePluckerLines

Where in *LBlock* every row represents a 3D line in the Plücker notation. And this function is based on the Function 4.6, which extracts the footpoint of the distance of the line from the origin based on the Plücker notation theroy in Section 3.2, and the direction of the line in space.

```
function [point, direction] = getPointDirectionFromPluckerLine(
    lineExtracted)
```

Listing 4.6: Function getPointDirectionFromPluckerLine

The plane of the laser is then determined, in terms of direction cosines, as the eigenvector associated with the smallest eigenvalue of the correlation matrix of the directions determined in the previous step. Moreover, the final parameter, associated with the distance of the plane from the origin, is obtained by projecting the point on the line determined earlier onto the normal vector of the plane. Therefore, the parameters of the plane become:

```
laserPlane = [PlaneNormal; -averageDistance];
```

4.2.5. Reconstruction of 3D Points

The process of determining the 3D coordinates of a point within the image (associated with the laser line) is accomplished through the utilization of Function 4.7,

```
function [Point] = get3DPointThroughLaserPlaneWithReferenceSystem(
    point2D, cameraParams, LaserPlane, referenceRotation,
    referenceTranslation, offset)
```

Listing 4.7: Function get3DPointThroughLaserPlaneWithReferenceSystem

Where the parameter `offset` is related to the movement of the conveyor belt between different frames and is used to reconstruct the profile of objects in motion on the belt. It can be adopted in case of a displacement of the global reference system is needed. Set the point in the 3D camera frame. This is analogous to assuming that the camera is located at the origin, so the reference rotation and translation become null: `P = K[eye(3) ones(3,1)]`, then `x = P * X -> P = inv(K) * x`. In Function 4.7, it is depicted as:

```
scaledPoint3D = (cameraParams.IntrinsicMatrix') \ [point2D 1]';
```

And in Function 4.7, the input parameter `LaserPlane` is given in the global reference system, so, in order to identify it in the camera coordinate system, it must be

divided by `Href' = [referenceRotation referenceTranslation; [0 0 0 1]]'`. It is represented as shown below:

```
LaserPlaneFromCamera = Href' \ LaserPlane;
```

The formula `a*lambda*x+b*lambda*y+c*lambda*z+d=0 -> lamda=-d/(ax+by+cz)` is then employed to determine the 3D intersection point, and its evaluation is carried out in the global reference system:

```
intersectionPoint = scaledPoint3D * (-LaserPlaneFromCamera(4) /
(scaledPoint3D' * LaserPlaneFromCamera(1:3)));
Point = Href \ [intersectionPoint; 1];
```

4.3. Simulation and Experimental Results

The constituent elements described above have been seamlessly integrated into the script *"FullReconstruction.m"* which processes a sequence of images depicting a simulated log which displacement between frames and employs the Function 4.7 to reconstruct its profile.

Now it is essential to choose a three-dimensional polygonal complex object as a target for algorithm validation. In this context, the trunk is selected as the target object. And the modeling model of this chosen target is depicted in Figure 4.10. The trunk model represents a real-world object, using a realistic object ensures that the algorithm is tested in conditions similar to its intended application. Moreover, the trunk typically exhibit complex geometric shapes with irregular surfaces. Calibrating the camera and laser line with such a complex object challenges the algorithm to handle diverse and non-uniform surfaces, making the calibration more robust.

Following that, in order to perform 3D point reconstruction of the trunk model, the laser line is "cut" on the trunk model. It serves as part of the input for Function 4.7 and offers essential data support for the execution of the script *"FullReconstruction.m"*. In this simulation, the laser line "cut" 40 times at various locations on the same trunk model. These 40 images can be found in the folder *"reconstructionTrunk"*, with Figure 4.11 displaying four of them.

The ultimate result is shown in Figure 4.12. It can be seen from the figure that the measured data points marked with "+" in various colors collectively form the three-dimensional reconstruction of the trunk model. It's important to highlight that in this simulation, all measurement values must be acquired in a specific reference system (the conveyor belt) Consequently, all measurement values are transformed into this reference

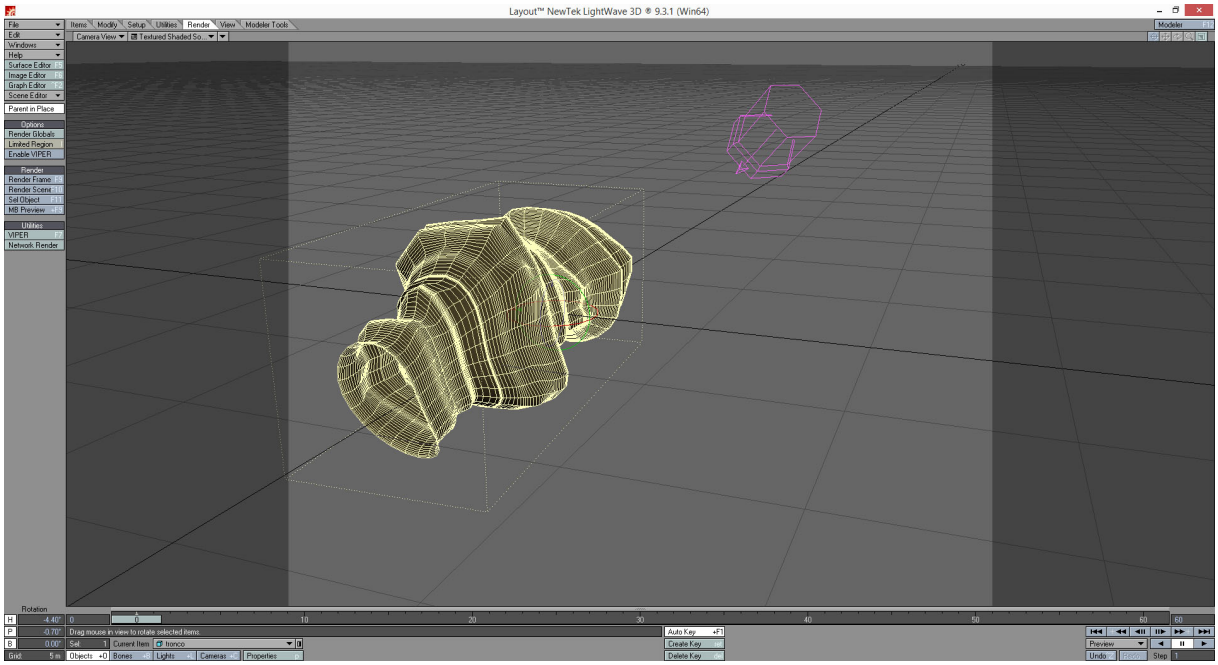

(a) Modeling Procedure

(b) Modeling Outcomes

Figure 4.10: Modeling of The Trunk.

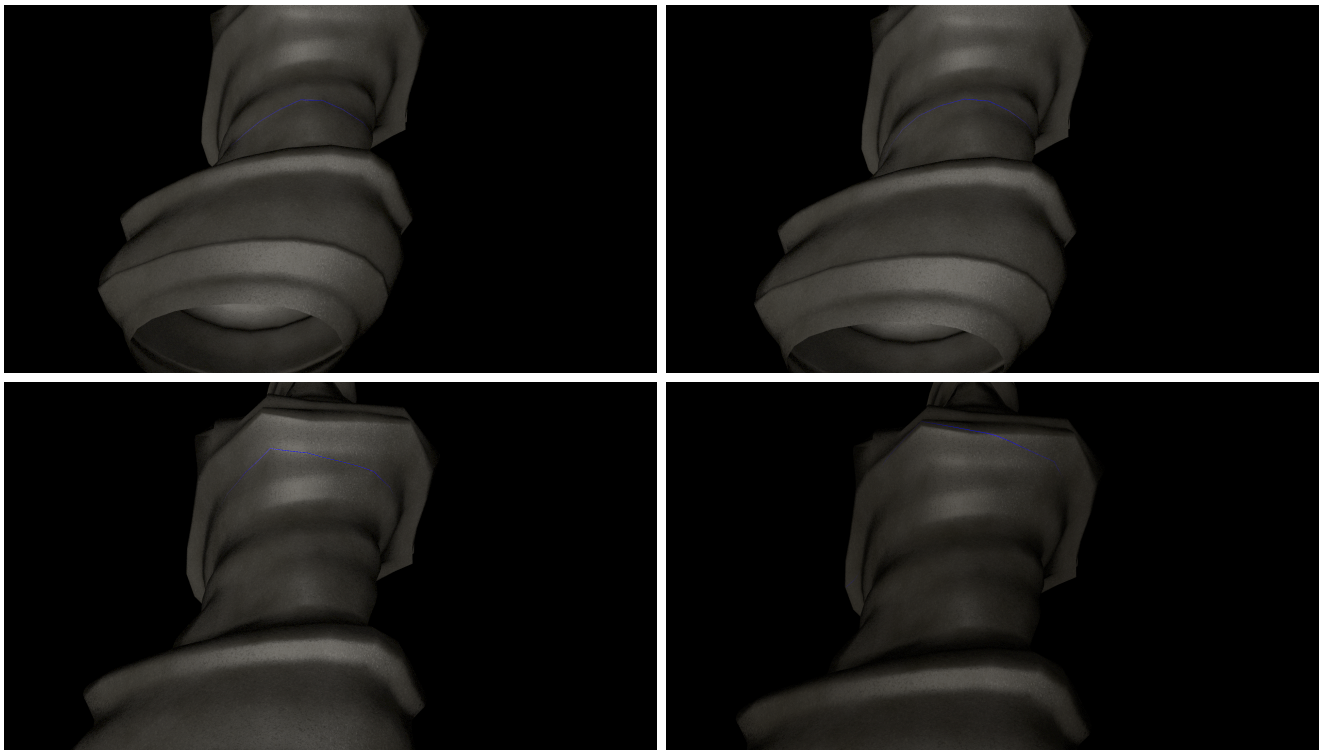

Figure 4.11: Modeling of The Trunk and The Laser Line.

frame, which aligns with the initial checkerboard reference frame coplanar with the conveyor belt.

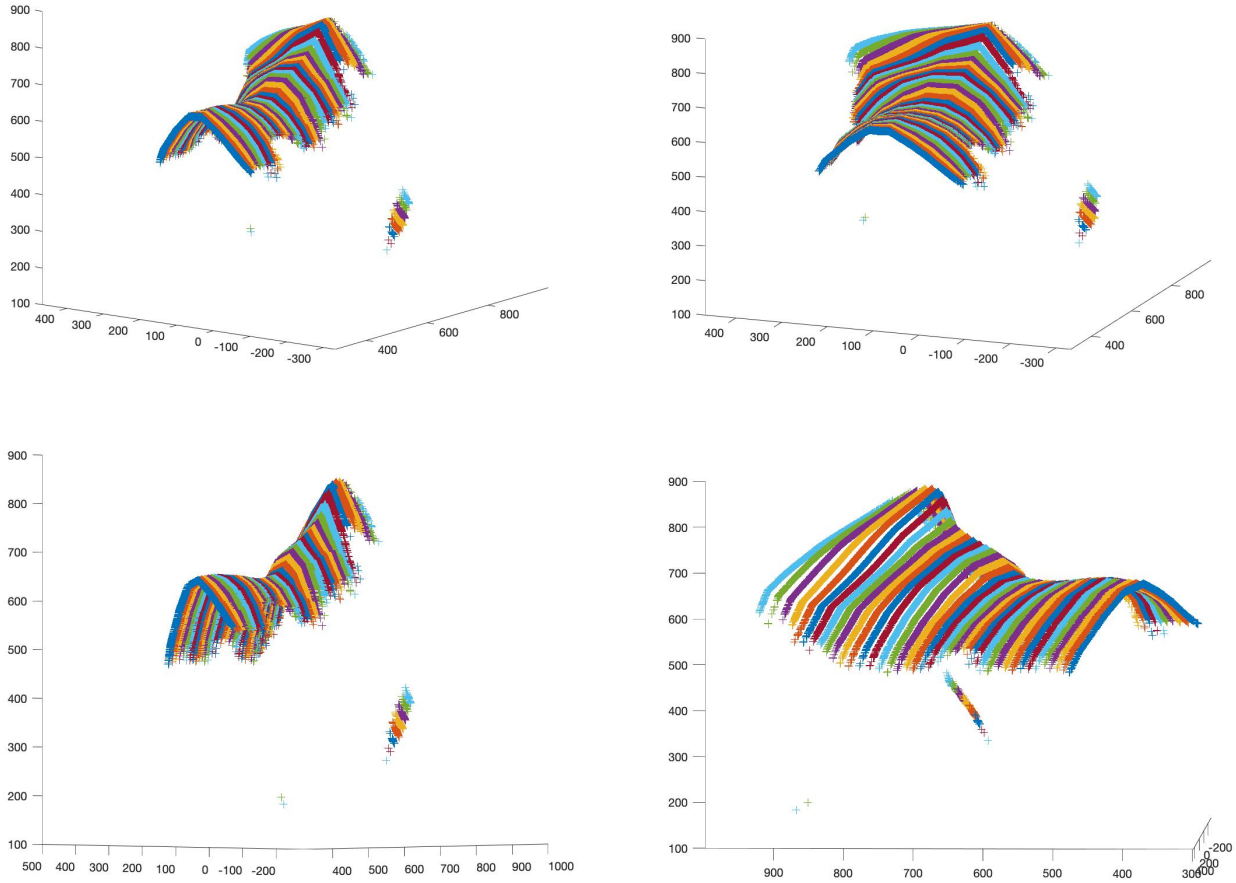

Figure 4.12: 3D Reconstruction Simulation of The Trunk.

5 | Conclusions and Future Developments

In this thesis, a novel approach for Camera-Laser line calibration has been presented, which is a fundamental task in computer vision with a wide range of applications, from 3D reconstruction to robotics. The approach builds upon the principles of Plücker line parameter extraction, laser plane determination, and 3D point reconstruction, offering a robust and versatile solution.

While the current framework presents a valuable contribution forward in the field of Camera-Laser line calibration, there are numerous exciting prospects for future research and development that can further augment and extend this work: Integrating this framework with specialized hardware, such as 3D cameras and LiDAR systems, can enhance the accuracy and versatility of the approach, making it suitable for a wider range of scenarios; The integration of machine learning techniques for object recognition, line detection and scene understanding can further augment the precision, speed and adaptability of the calibration and the 3D reconstruction process; Optimizing the framework for real-time processing is essential for applications demanding rapid decision-making, such as autonomous navigation and surveillance systems; Designing an intuitive user interface for this tool can democratize its usage, enabling non-experts to leverage its capabilities effectively; Investigating how this approach can be applied in different domains, such as medical imaging or archaeological surveys, could reveal new opportunities for innovation. In summary, I am eager to witness how this work will inspire further research and innovation, ultimately leading to groundbreaking solutions with far-reaching applications in the world of computer vision and beyond.

Bibliography

[1] R. Hartley and A. Zisserman, *Multiple view geometry in computer vision*. Cambridge university press, 2003.

[2] R. Y. Tsai, "An efficient and accurate camera calibration technique for 3d machine vision," in *Computer Vision and Pattern Recognition*, 1986.

[3] R. Y. Tsai, "A versatile camera calibration technique for high-accuracy 3d machine vision metrology using off-the-shelf tv cameras and lenses," *IEEE J. Robotics Autom.*, vol. 3, pp. 323–344, 1987.

[4] Z. Zhang, "A flexible new technique for camera calibration," *IEEE Transactions on Pattern Analysis and Machine Intelligence*, vol. 22, no. 11, pp. 1330–1334, 2000.

[5] H. Schilling, M. Diebold, M. Gutsche, and B. Jähne, "On the design of a fractal calibration pattern for improved camera calibration," *tm - Technisches Messen*, vol. 84, no. 7-8, pp. 440–451, 2017.

[6] T. Schöps, V. Larsson, M. Pollefeys, and T. Sattler, "Why having 10,000 parameters in your camera model is better than twelve," in *2020 IEEE/CVF Conference on Computer Vision and Pattern Recognition (CVPR)*, pp. 2532–2541, 2020.

[7] M. R. Hannemose, J. Wilm, and J. R. Frisvad, "Superaccurate camera calibration via inverse rendering," in *Optical Metrology*, 2019.

[8] C. Gao and J. R. Spletzer, "On-line calibration of multiple lidars on a mobile vehicle platform," in *2010 IEEE International Conference on Robotics and Automation*, pp. 279–284, 2010.

[9] T. Svoboda, D. Martinec, and T. Pajdla, "A convenient multicamera self-calibration for virtual environments," *Presence: Teleoperators & Virtual Environments*, vol. 14, pp. 407–422, 2005.

[10] S. Wasielewski and O. Strauss, "Calibration of a multi-sensor system laser rangefinder/camera," in *Proceedings of the Intelligent Vehicles '95. Symposium*, pp. 472–477, 1995.

[11] Q. Zhang and R. Pless, "Extrinsic calibration of a camera and laser range finder (improves camera calibration)," in *2004 IEEE/RSJ International Conference on Intelligent Robots and Systems (IROS) (IEEE Cat. No.04CH37566)*, vol. 3, pp. 2301–2306 vol.3, 2004.

[12] L. Zhou, "A new minimal solution for the extrinsic calibration of a 2d lidar and a camera using three plane-line correspondences," *IEEE Sensors Journal*, vol. 14, no. 2, pp. 442–454, 2014.

[13] F. Vasconcelos, J. P. Barreto, and U. Nunes, "A minimal solution for the extrinsic calibration of a camera and a laser-rangefinder," *IEEE Transactions on Pattern Analysis and Machine Intelligence*, vol. 34, no. 11, pp. 2097–2107, 2012.

[14] Z. Hu, Y. Li, N. Li, and B. Zhao, "Extrinsic calibration of 2-d laser rangefinder and camera from single shot based on minimal solution," *IEEE Transactions on Instrumentation and Measurement*, vol. 65, no. 4, pp. 915–929, 2016.

[15] R. Unnikrishnan and M. Hebert, "Fast extrinsic calibration of a laser rangefinder to a camera," *Robotics Institute, Pittsburgh, PA, Tech. Rep. CMU-RI-TR-05-09*, 2005.

[16] A. Geiger, F. Moosmann, O. Car, and B. Schuster, "Automatic camera and range sensor calibration using a single shot," in *2012 IEEE International Conference on Robotics and Automation*, pp. 3936–3943, 2012.

[17] S. Sim, J. Sock, and K. H. Kwak, "Indirect correspondence-based robust extrinsic calibration of lidar and camera," *Sensors (Basel, Switzerland)*, vol. 16, 2016.

[18] C. Guindel, J. Beltrán, D. Martín, and F. T. García, "Automatic extrinsic calibration for lidar-stereo vehicle sensor setups," *2017 IEEE 20th International Conference on Intelligent Transportation Systems (ITSC)*, pp. 1–6, 2017.

[19] S. A. Rodriguez F., V. Fremont, and P. Bonnifait, "Extrinsic calibration between a multi-layer lidar and a camera," in *2008 IEEE International Conference on Multisensor Fusion and Integration for Intelligent Systems*, pp. 214–219, 2008.

[20] H. Alismail, L. D. Baker, and B. Browning, "Automatic calibration of a range sensor and camera system," *2012 Second International Conference on 3D Imaging, Modeling, Processing, Visualization & Transmission*, pp. 286–292, 2012.

[21] V. Lepetit, F. Moreno-Noguer, and P. Fua, "Epnp: An accurate o(n) solution to the pnp problem," *International Journal of Computer Vision*, vol. 81, pp. 155–166, 2009.

[22] Y. Abdel-Aziz and H. Karara, "Direct linear transformation into object space co-

ordinates in close-range photogrammetry," in *In Proceedings of the Symposium on Close-Range Photogrammetry*, pp. 1–18, 1971.

[23] B. Triggs, P. F. McLauchlan, R. I. Hartley, and A. W. Fitzgibbon, "Bundle adjustment — a modern synthesis," in *Vision Algorithms: Theory and Practice* (B. Triggs, A. Zisserman, and R. Szeliski, eds.), (Berlin, Heidelberg), pp. 298–372, Springer Berlin Heidelberg, 2000.

[24] P. Tulsuk, P. Srestasathiern, M. Ruchanurucks, T. Phatrapornnant, and H. Nagahashi, "A novel method for extrinsic parameters estimation between a single-line scan lidar and a camera," in *2014 IEEE Intelligent Vehicles Symposium Proceedings*, pp. 781–786, 2014.

[25] D. Scaramuzza, A. Harati, and R. Y. Siegwart, "Extrinsic self calibration of a camera and a 3d laser range finder from natural scenes," *2007 IEEE/RSJ International Conference on Intelligent Robots and Systems*, pp. 4164–4169, 2007.

[26] R. Gomez-Ojeda, J. Briales, E. Fernandez-Moral, and J. Gonzalez-Jimenez, "Extrinsic calibration of a 2d laser-rangefinder and a camera based on scene corners," in *2015 IEEE International Conference on Robotics and Automation (ICRA)*, pp. 3611–3616, 2015.

[27] C. Rodriguez Garavito, A. Ponz, F. Garcia, D. Martín Gómez, A. de la Escalera, and J. Armingol, "Automatic laser and camera extrinsic calibration for data fusion using road plane," in *FUSION 2014 - 17th International Conference on Information Fusion*, 07 2014.

[28] J. Fan, F. Jing, Z. Fang, and Z. Liang, "A simple calibration method of structured light plane parameters for welding robots," in *2016 35th Chinese Control Conference (CCC)*, pp. 6127–6132, 2016.

[29] C. Che and J. Ni, "A ball-target-based extrinsic calibration technique for high-accuracy 3-d metrology using off-the-shelf laser-stripe sensors," *Precision Engineering*, vol. 24, no. 3, pp. 210–219, 2000.

[30] Z. Xie, X. Wang, and S. Chi, "Simultaneous calibration of the intrinsic and extrinsic parameters of structured-light sensors," *Optics and Lasers in Engineering*, vol. 58, pp. 9–18, 2014.

[31] Z. Wei, M. Xie, and G. Zhang, "Calibration method for line structured light vision sensor based on vanish points and lines," in *2010 20th International Conference on Pattern Recognition*, pp. 794–797, 2010.

[32] G. Xu, A. Zheng, X. Li, and J. Su, "Optimization solution of laser plane generated from maximum likelihood estimation of projection plane," *Sensors and Materials*, vol. 30, no. 5, p. 1155 – 1164, 2018. Cited by: 3; All Open Access, Gold Open Access.

[33] M. A. Sutton, J.-J. Orteu, and H. W. Schreier, *Image correlation for shape, motion and deformation measurements : basic concepts, theory and applications*. Springer, 2009.

[34] G. Besnard, *Caractérisation et quantification de surfaces par stéréocorrélation pour des essais mécaniques du quasi statique à la dynamique ultra-rapide*. Theses, École normale supérieure de Cachan - ENS Cachan, Mar. 2010.

List of Figures

List of Tables

List of Symbols